Peripheral sensory neurons and non-neuronal cells express functional Piezo1 that is activated in peripheral nerve injury-induced neuropathic pain

Abbreviated Title: Peripheral nerve Piezo1 is activated following neuropathic pain

Seung Min Shin[1], Brandon Itson-Zoske[1], Fan Fan[2], Cheryl L. Stucky[3], Quinn H. Hogan[1], and Hongwei Yu[1*]

1. Department of Anesthesiology, Medical College of Wisconsin, Milwaukee, WI 53226
2. Department of Pharmacology and Toxicology, Mississippi University Medical Center, Jackson, Mississippi 39216
3. Department of Cell Biology, Neurobiology, and Anatomy, Medical College of Wisconsin, Milwaukee, WI 53226

*** Correspondence author**: hyu@mcw.edu, phone: 414-955-5745

Conflict of interest statement: The authors declare no competing financial interests.

Acknowledgments: This research was supported by a grant from National Institutes of Health grant R61NS116203 (to HY and QH), a National Institutes of Health grants NS108278 (to CLS), and an MCW NRC grant FP00016291 (to HY). The authors thanks Mr. Michael Pereckas, MCW proteomics core, for his help in performing LC-MS/MS and protein identification.

Abstract

Here, we present evidence showing Piezo1 expression in the primary sensory neurons (PSNs) and non-neuronal cells of rat peripheral nervous system. Using a knockdown/knockout validated antibody, we detected Piezo1 immunoreactivity (IR) in ~80% of PSNs of rat dorsal root ganglia (DRG) with higher IR density in the small- and medium-sized neurons, and within axons extending to both central presynaptic terminals innervating to the spinal dorsal horn and peripheral cutaneous sensory terminals in the skin. Piezo-IR was clearly identified in DRG perineuronal glia, including satellite glial cells (SGCs) and non-myelinating Schwann cells; in sciatic nerve Schwann cells surrounding the axons and cutaneous afferent endings; and in skin epidermal Merkel cells and melanocytes. Neuronal and non-neuronal Piezo1 channels were functional, since various cells (dissociated PSNs and SGCs from DRGs, isolated Schwann cells, and primary human melanocytes) exhibited a robust response to Piezo1 agonist Yoda1 by an increase of intracellular Ca^{2+} concentration ($[Ca^{2+}]_i$). These responses were abolished by Piezo1 antagonist GsMTx4. Immunoblots showed elevated Piezo1 protein in DRG proximal to peripheral nerve injury-induced painful neuropathy, while PSNs and SGCs from rats with neuropathic pain showed greater Yuda1-evoked elevation of $[Ca^{2+}]_i$ and an increased frequency of cells responding to Yoda1, compared to controls. Ipsilateral sciatic nerve application of GsMTx4 alleviated mechanical hypersensitivity following nerve injury. Overall, our data show that Piezo1 is widely expressed by the neuronal and non-neuronal cells in the peripheral sensory pathways and that painful nerve injury is associated with activation of Piezo1 in PSNs and peripheral glia cells.

Key words: Piezo1; Peripheral nervous system; Dorsal root ganglia; Sensory neurons; Satellite glial cells; Schwann cells; Pain

Introduction

Piezo channels, including Piezo1 and Piezo2, are *bona fide* mechanosensitive channels (MSCs) that are expressed widely throughout the body of mammals [18, 59]. These channels provide critical functions as constitutive *Piezo1* and *2* knockout mice die during embryogenesis and at birth, respectively [58, 60]. In humans, mutations in the genes encoding *PIEZO* channels are not life-threatening but lead to multiple hereditary human diseases, such as such as xerocytosis, arthrogryposis, and lymphedema [4]. Lack of painful reactions to innocuous touch after skin inflammation is reported in human with the mutations of *PIEZO2* but not *PIEZO1* [14]. Piezo1 is considered as a polymodal sensor of diverse mechanical forces primarily expressed in the non-sensory tissues exposed to fluid pressure and flow, whereas Piezo2 is predominantly found in the PSNs of sensory ganglia and cutaneous Merkel cells that respond to mechanical touch specifically [91]. A search of the publicly available datasets in Human Protein Atlas (https://www.proteinatlas.org), the deposited data in the GenBank GEO Profiles (https://www.ncbi.nlm.nih.gov/geoprofiles/), and published literature indicate presence of Piezo1 transcripts in total DRG and trigeminal ganglia (TG), isolated DRG/TG neurons, human Schwann cells, spinal cord dorsal horn and motor neurons, and brain [22, 24, 43].

Recent studies provide new insights into the potential roles of Piezo1 in peripheral sensory and nociceptive mechanobiology. RNAscope identifies Piezo1 in the DRG- and TG-PSNs of mice and mole, which is highly enriched in the smaller-sized PSNs, and also detected in the perineuronal glial cells of mice DRG [83]. Piezo1 protein was detected in rat and mouse DRG by immunoblots [16, 68]. Application of the Piezo1-selective agonist Yoda1 to dissociated PSNs

and recording mechanically evoked currents both reveal functional Piezo1[47, 62]. Piezo1 is also expressed in keratinocytes, where it may contribute to cutaneous nociception by modulating sensory afferent firing [77, 78]. Additionally, selective ablation of skin keratinocyte-Piezo1 in mice reduces responsiveness to non-noxious and noxious mechanical stimuli but spares responses to thermal stimuli [50]. Systemic administration of a Piezo1-inhibiting tarantula spider toxin (GsMTx4, a nonspecific Piezo1 antagonist) relieves mechanical hypersensitivity in mice from both peripheral nerve injury and inflammation [55], while intra-articular injection of GsMTx4 relieves hypersensitivity in osteoarthritic mice [30]. Finally, hindpaw intradermal Yoda1 causes prolonged hyperalgesia [83] and paw attending responses [50] while injection of GsMTx4 reverses the mechanical hyperalgesia induced by intradermal injection of inflammatory mediators [3]. Although analgesic effects of GsMTx4 could be due to inhibition of multiple MSCs, these observations together suggest a possibility that Piezo1 may contribute to peripheral nerve nociceptive mechanobiology.

Piezo1 protein expression and cell specificity in rat peripheral nerves have not been systematically studied. On pursuing the therapeutic potentials targeting Piezos for chronic pain in rat models, this study was designed to determine the Piezo1 expression in rat peripheral sensory pathway. Specifically, we examined the Piezo1 protein expression and cell specificity in DRG, sciatic nerve, afferent peripheral and central terminals, and hindpaw skin. Functional Piezo1 was tested by Yoda1 stimulated increases of intracellular calcium ($[Ca^{2+}]_i$). Piezo1 protein expression in DRG was characterized in rat models of peripheral nerve injury-induced painful neuropathy. Our data identifies Piezo1 protein expression in the PSNs and non-neuronal glial cells. Peripheral PSNs and perineuronal glial cells express functional Piezo1 that is activated following neuropathic

pain. These results suggest that Piezo1 plays roles in peripheral mechanosensory processing that could contribute chronic pain pathogenesis.

Materials and Methods

Animals

Adult male Sprague Dawley (SD) rats (6-8 week old, Charles River Laboratories, Wilmington, MA) and male mice in C57BL/6 background with keratinocyte-selective Piezo1 null ($k14^{Cre}/Piezo1^{fl/fl}$) and their wild type littermates at the age of ~6 month-old [50] were used. All animal experiments were performed with the approval of the Medical College of Wisconsin Institutional Animal Care and Use Committee in accordance with the National Institutes of Health Guidelines for the Care and Use of Laboratory Animals. Animals were housed individually in a room maintained at constant temperature (22±0.5°C) and relative humidity (60±15%) with an alternating 12h light-dark cycle, were given access to water and food *ad libitum* throughout the experiment, and all efforts were made to minimize suffering and the numbers of animal used. For tissue harvest euthanasia, animals were deeply anesthetized by isoflurane followed by decapitation with a well-maintained guillotine.

Rat pain models and sensory behavior testing

Peripheral nerve injury models. Two neuropathic pain rat models by spared nerve injury (SNI) and tibial nerve injury (TNI) were generated as we described previously [68]. To generated unilateral right SNI or TNI, after surgical exposure, the tibial and common peroneal (SNI, leaving sural nerve intact) or tibial nerve alone (TNI, leaving common peroneal and sural nerve intact) were individually ligated and severed distally to the ligature, and 2–3mm of ligated nerve was removed distal of the ligation. After surgery, muscle and skin were closed using 4.0

monofilament nylon sutures and wound clips. Sham-operated rats were subjected to all preceding procedures in the same manner as pain models but without nerve ligation and transection.

Mechanical allodynia and hyperalgesia: Mechanical allodynia was assessed as the mechanical withdrawal threshold (von Frey, vF) and hyperalgesia was identified by noxious punctate mechanical stimulation (Pin test), as we described previously [23]. In brief, vF test was performed by applying the calibrated monofilaments (Patterson Medical, Bolingbrook, IL) to the plantar surface of the hindpaw. Beginning with the 2.8 g filament, if a response was observed, the next smaller filament was applied, and if no response was observed, the next larger was applied, until a reversal occurred, defined as a withdrawal after a previous lack of withdrawal, or vice versa. Following a reversal event, four more stimulations were performed following the same pattern. The forces of the filaments before and after the reversal, and the four filaments applied following the reversal, were used to calculate the 50% withdrawal threshold [23]. Rats not responding to any filament were assigned a score of 25 g. Pin test was performed using the point of a 22 g spinal anesthesia needle that was applied to the center of the hindpaw with enough force to indent the skin but not puncture it. Five applications were separated by at least 10s each, which was repeated after 2 min, making a total of 10 touches. For each application, the induced behavior was either a very brisk, simple withdrawal with immediate return of the foot to the cage floor, or a sustained elevation with grooming behavior that included licking and chewing, and possibly shaking, which lasted at least 1s. This latter behavior was referred to as hyperalgesic behavior [89], which is specifically associated with place avoidance. Hyperalgesia was quantified by tabulating hyperalgesia responses as a percentage of total touches.

Tissue harvest for immunohistochemistry (IHC) and immunoblots

After transcardial perfusion with 100ml PBS in rats and 40ml in mice, lumbar (L) 4 and 5 DRG, lumbar segment spinal cord, sciatic nerve segment proximal to the sciatic bifurcation, brain, and hindpaw glabrous and hairy skin tissues were dissected, and fixed in Richard-Allan Scientific™ Buffered Zinc Formalin (ThermoFisher, Rockford, IL) overnight (~15 hr) for DRG, sciatic nerves, and skins; and 24 hr for spinal cord and brain, followed by processing for paraffin embedment. Serial sections at 5μm thickness, oriented coronally for brain, sagittally for DRG and sciatic nerve, axially for spinal cord, and perpendicular to the skin surface for skin tissues, were prepared and mounted on positively charged SuperForst microscope slides (ThermoFisher). For cryosection, fixed tissues were cryoprotected by overnight infiltration with 30% sucrose solution in 1x phosphate-buffered saline (PBS), followed by mounting in OCT embedding compound, and freezing to -80°C. Fifteen μm thickness cryosections were prepared on a cryostat (Leica CM1950, Kyoto, Japan) and air-dried for 24 hr. For western blot experiments, L4/L5 DRG were removed, snap frozen in liquid nitrogen, and stored at −80°C for extraction of protein.

Primary cell culture (all from rats) and cell lines

DRG dissociated culture [67]: In brief, the L4/5 DRG were rapidly harvested from the isoflurane anesthetized rats and were incubated in 0.01% blendzyme 2 (Roche Diagnostics, Madison, WI) for 30 min followed by incubation in 0.25% trypsin and 0.125% DNase for 30 min, both dissolved in Dulbecco's modified Eagle's medium/F12 (DMEM/F12) with glutaMAX (ThermoFisher). After exposure to 0.1% trypsin inhibitor and centrifugation, the pellet was gently triturated, and dissociated cells were plated onto 5% laminin-coated glass coverslips (ThermoFisher) and maintained at 37°C in humidified 95% air and 5% CO_2 for 3 h in Neural

basal media A (ThermoFisher) plus 0.5 μM glutamine, and were studied by Ca^{2+} imaging no later than 6 h after harvest.

Sciatic nerve (SN) Schwann cell isolation: The relevant steps required for nerve processing, enzymatic dissociation, and cell plating using the SN from one adult male rat was previously described, with minor modifications [5, 67]. In brief, bilateral sciatic nerves were harvested and attached adipose and muscular tissue stripped off using fine forceps. Subsequently, the desheathed inner nerve elements were collected for enzymatic digestion for 2hr as described in DRG dissociated culture. The end products of enzymatic digestion were filtered and subsequently collected by centrifugation. isolated rat SCs were cultured in Schwann cell medium (Edina) for 3-4 days before Ca^{2+} imaging experiments

Spinal cord dorsal horn (SDH) glia isolation: Spinal DH glial cells isolation was performed essentially the same as DRG dissociation. The rats (male, one-month old) were killed by decapitation during anesthesia. The vertebral column was removed and cut into slices and collected in Petri dishes filled with cold DMEM/F12. After removing the vertebral arch, dorsal parts of the spinal cord were extracted, cleaned from surrounding spinal meninges, and collected in cold DMEM/F12. All spinal dorsal horn slices were transferred into an enzyme mix for as DRG dissociation. After enzymatic digestion for 30 min, cells were dissociated mechanically, washed, and precipitated by centrifugation (2 min with 2000 rpm). The supernatant was removed, and cells were re-suspended in cultural medium consisting of Neurobasal A supplemented with 2% B27 and 10% FBS and cultured on poly-L-lysine (0.01mg/ml) coated glass coverslips for 12hr before Ca^{2+} imaging experiments.

Cell lines: As a second source of Schwann cells, primary Schwann cells isolated from human spinal nerve were obtained from Neuromics (HMP303, Edina, MN). Primary adult human

epidermal melanocytes were purchased from ThermoFisher (C0245C). Human SCs were cultured in Schwann cell medium (Edina), and human epidermal melanocytes cultured in Medium 254 with melanocyte growth supplement (ThermoFisher), according to manufacturer's protocols. Neuronal NG108-15 (NG108 cells), NSC34 spinal cord motor neuron-like cells and C6 astrocytes were obtained from ATCC (Manassas, VA). Rat DRG-neuronal 50B11 cells (50B11) were used as reported previously [93]. These cells were cultured by a standard protocol using Dulbecco's modified Eagle's medium (DMED) supplemented with 10% FBS and antibiotics (ThermoFisher). All cells were grown at 37°C and in 5% CO_2 in a humidified incubator.

Microfluorimetric Ca^{2+} imaging

Determination of $[Ca^{2+}]_i$ was performed using Fura-2 based microfluorimetry and imaging analysis as we previously described [67]. Unless otherwise specified, the agents were obtained from Sigma-Aldrich. Dissociated DRG neurons, SGCs, sciatic nerve SCs, and DH glia from naïve rats, as well as human melanocytes, NSC34 cells, 50B11 cells, and C6 astrocytes, were evaluated for responses to Yoda1 at different concentrations (μM) in extracellular buffer to determine the dose response relationship from at least three different cultures.

For measurement of $[Ca^{2+}]_i$, cells cultured on coverslips were loaded with Fura-2-AM (5μM, ThermoFisher) and maintained in 25°C Tyrode's solution containing (in mM): NaCl 140, KCl 4, $CaCl_2$ 2, glucose 10, $MgCl_2$ 2, and 4-(2-hydroxyethyl)-1- piperazineethanesulfonic acid (HEPES) 10, with an osmolarity of 297 to 300 mOsm and pH 7.4. After 30 min, they were washed three times with regular Tyrode's solution and left in a dark environment for de-

esterification for 30 min and then mounted onto a 0.5ml recording chamber that was constantly superfused by a gravity-driven bath flow at a rate of 3 ml/min. Agents were delivered by directed microperfusion controlled by a computerized valve system through a 500μm-diameter hollow quartz fiber 300 μm upstream from the chamber. This flow completely displaced the bath solution, and constant flow was maintained by delivery of bath solution when specific agents were not being administered. Solution changes were achieved within 200ms. The fluorophore was excited alternately with 340 nm and 380 nm wavelength illumination (150 W xenon, Lambda DG-4; Sutter), and images were acquired at 510 nm using a cooled 12 bit digital camera (Coolsnap fx; Photometrics) and inverted microscope (Diaphot 200; Nikon Instruments) through a 20x or 40x Fluor oil-immersion objective. Cells were imaged to monitor Ca^{2+} responses to Yoda1 with difference concentration and total DMSO concentration was kept equal to and below 1% for all tested Yoda concentrations. $[Ca^{2+}]_i$ was evaluated as the ratio of emission in response to excitation at 340 and 380 nm, expressed as the 340/380 nm fluorescence emission ratio ($R_{340/380}$) that is directly correlated to the amount of intracellular calcium [26]. A ≥30% increase in $R_{340/380}$ from baseline after superfusion with yoda1 was considered a positive response for all cells recorded [50]. Response of neurons to 50 mM KCl solution at the end of each protocol was used as a criterion for identifying viable neurons, and similarly for the response of SGCs to 10 μM ATP. Plasma membrane Ca^{2+}-ATPase influence was eliminated by applying Tyrode's with pH 8.8 during depolarization, while stable cytoplasmic $[Ca^{2+}]_c$ was maintained by simultaneously reducing bath Ca^{2+} concentration to 0.25mM [21].

Immunofluorescent staining

Previously established protocols were adopted [68]. For immunocytochemistry (ICC), the cultured cells were fixed in 2% paraformaldehyde (PFA) in 1xPBS solution for 5 min. For IHC, the formalin-fixed, paraffin-embedded (FFPE) tissue sections were deparaffinized in xylene, rehydrated through graded alcohol, and treated by heat-induced antigen epitope retrieval in 10mM citrate buffer, pH 6.0; cryosections were treated by 3% hydrogen peroxide for 10 min to block endogenous peroxidase activity. Non-specific binding was reduced by incubating the sections for 30 min with a solution of 5% BSA in PBS solution. Samples were first immunolabeled with the selected primary antibodies in a humid atmosphere overnight at 4°C (**Table 1**). All antibodies were diluted in 1 x PBS, containing 0.05% Triton X-100 and 5% bovine serum albumin (BSA). Normal immunoglobulin G (IgG from the same species as the first antibody, **Table 1**) was replaced for the first antibody as the negative controls. The appropriate fluorophore-conjugated (Alexa 488 or Alexa 594, 1:2000) secondary antibodies (Jackson ImmunoResearch, West Grove, PA) were used to reveal immune complexes. Afterward, the sections were rinsed for 5 min in PBS and either processed for a colabeling of primary and secondary antibodies or coverslipped under *Shur/Mount* mounting medium (ThermoFisher). To control for false-positive results attributable to cross-binding in double-label combinations, each primary antibody was raised in a different species was used. To stain nuclei, 1.0μg/ml Hoechst33342 (Hoechst, ThermoFisher) was added to the secondary antibody mixture. The immunostaining was examined, and images captured using a Nikon TE2000-S fluorescence microscope (El Segundo, CA) with filters suitable for selectively detecting the green and red fluorescence using a QuantiFire digital camera (Optronics, Ontario, NY). For double label colocalization, images from the same specimen but showing different antigen signals were overlaid by digitally merging the captured images.

Two different rabbit polyclonal Piezo1 antibodies were obtained from Proteintech (Rosemont, IL) and from Alomone (Jerusalem, Israel), respectively. The specificity of these two Piezo1 antibodies has been validated in knockout (KO) tissues, in cells with RNAi-mediated Piezo1 knockdown (KD), and are widely used to detect Piezo1 expression by IHC and immunoblots [13, 17, 42, 71, 73, 84]. The Alomone Piezo1 antibody was used for all IHC and immunoblots, while Proteintech Piezo1 antibody used for ICC on the human melanocytes since Alomone Piezo1 antibody does not detect on human Piezo1 according to the datasheet from the vendor. To control for Piezo1 immunostaining, representative sections were processed in the same way as described but using non-immune rabbit IgG instead of the Piezo1 primary antibody in the incubation. The specificities of the other antibodies used in this study have been previously confirmed, and the specificity of secondary antibodies was tested with omission of the primary antibodies, which has always resulted in absence of immunostaining [68].

Quantification of immunostaining

Positive marker antibody immunostaining was defined as the cells having a fluorescence intensity greater than the average background fluorescence plus 2 standard deviations of the cells in a section of negative control (first antibody omitted) under identical acquisition parameters (n=10 for different markers), identified by Hoechst counterstain at a different wavelength [92].

Intensity correlation analysis (ICA) was performed to determine colocalization of Piezo1 with neuronal plasma membrane (PM) marker sodium/potassium ATPase 1 alpha (NKA1a) and SGC marker glial fibrillary acidic protein (GFAP), as previously described using an ImageJ 1.46r

software plugin colocalization analysis module (http://imagej.nih.gov/ij) [41, 67, 95]. In brief, fluorescence intensity was quantified in matched region of interest (the green and red colors varied in close synchrony) for each pair of images. Mean background was determined from areas outside the section regions and was subtracted from each file. On the basis of the algorithm, in an image where the intensities vary together, the product of the differences from the mean (PDM) will be positive. If the pixel intensities vary asynchronously (the channels are segregated), then most of the PDM will be negative. The intensity correlation quotient (ICQ) is based on the nonparametric sign-test analysis of the PDM values and is equal to the ratio of the number of positive PDM values to the total number of pixel values. The ICQ values are distributed between -0.5 and +0.5 by subtracting 0.5 from this ratio. In random staining, the ICQ approximates 0. In segregated staining, ICQ is less than 0, while for dependent staining, ICQ is greater than 0.

Immunoblot analysis of Piezo1 expression

DRG tissue lysates were prepared from the pooled L4/L5 DRG from TNI, SNI, and sham-operated rats using 1x RIPA ice-cold buffer (20 mm Tris-HCl pH 7.4, 150 mm NaCl, 1% Nonidet P-40, 1% sodium deoxycholate, 0.1% SDS, with 0.1% Triton X100 and protease inhibitor cocktail) and rotated at 4 °C for 1 h before the supernatant was extracted by centrifugation at 12,000 g at 4 °C for 5 min. Protein concentration was determined using Pierce BCA kit (ThermoFisher). Equivalent protein samples were size separated using 10% or 4-20% SDS-PAGE gels (Bio-Rad), transferred to Immun-Blot PVDF membranes (Bio-Rad), and blocked for 1 hr in 5% skim milk. In some experiments, the transferred PVDF membranes were cut into two halves along protein size 70kDa and were subsequently incubated overnight at 4°C with appropriate antibodies. Immunoreactive proteins were detected by Pierce enhanced

chemiluminescence (ThermoFisher) on a ChemiDoc Imaging system (Bio-Rad) after incubation for 1 hr with HRP-conjugated second antibodies (1:5000, Bio-Rad). ImageJ program was used for quantification.

Piezo1 co-immunoprecipitation (Co-IP) and protein identification by LC-MS/MS

The DRG lysates from naïve rats were incubated on ice for 10 min followed by centrifugation at 12,000g for 20 min at 4 °C to remove the insoluble fraction. The supernatant was transferred to a new tube, 50µl of which was saved as input, and the rest of the supernatant was precleared by incubation with 1mg 1xPBS pre-washed Dynabeads (Thermo Fisher Scientific) on a rotator at 4°C for 1h. To prepare the antibody-coupled beads, Piezo1 antibody (Alomone) was incubated together with washed Dynabeads (8µg antibody per mg beads used) in 1x PBS buffer with 0.1M citrate (pH 3.1) on a rotator at 4°C overnight. Controls were generated using washed beads not coupled to antibody but normal rabbit IgG. Following overnight incubation, the supernatant was collected and saved in a new tube. The Co-IP beads were washed three times in ice-cold 1xPBS buffer by gentle pipetting and directly boiled in 60 µl 1x SDS sample buffer at 95 °C for 10 min to elute protein complexes from the beads. Immunoprecipitated samples were separated by SDS-PAGE gel and stained with silver (Thermo Fisher Scientific). The stained gel regions of interests were excised, and in-gel trypsin digested as previously described [97]. Extracted tryptic peptides were analyzed by nano reversed-phase liquid chromatography tandem mass spectrometry (nLC-MS/MS) using a nanoACQUITY (Waters Corporation, Milford, MA, USA) online coupled with an Orbitrap Velos Pro hybrid ion trap mass spectrometer (Thermo Fisher Scientific). MS/MS spectra from the Piezo1 Co-IP experiment were searched and processed using the rat proteome database.

GsMTx4 subepineural sciatic nerve injection

Injection was performed in a blinded manner in which the operator was unaware of the content of the injectate. GsMTx4 was dissolved in saline to a 100 mM stock solution, stored at -20°C, diluted to desired concentrations with saline before use. It is reported that half of the total cross-section inside the sciatic nerve epineurium in human consists of non-neural connective tissue [48]. Rats at 3-wk after TNI induction were randomized into two groups and sciatic nerve injection was performed as previously described [29, 66]. In brief, after appropriate anesthesia was obtained by inhalation of 2% isoflurane, the ipsilateral sciatic nerves were exposed through a lateral incision of the middle thighs and division of the superficial fascia and muscle. Then 100 μl of the test dose of GsMTx4 was injected slowly, directly into subepineural space (beneath the clear fascia surrounding the nerve but outside the perineurium) through a 33-gauge needle, proximal to the sciatic bifurcation. The needle remained in place at the injection site for 1 additional min, before it was slowly removed. Control rats received sciatic nerve injection with 100 μl saline. The superficial muscle layer was sutured with 4-0 silk, and the wound was closed with metal clips. Ipsilateral hindpaw mechanical allodynia (vF) and hyperalgesia (Pin) were tested before and 15, 30, 45, 60, 120, and 180 min after the animal fully recovered from anesthesia, indicated by being fully alert with normal posture, balance and gait, which typically required 3~5 minutes following termination of the anesthetic administration.

Statistical analyses

Statistical analysis was performed with GraphPad PRISM 6 (GraphPad Software, San Diego, CA). The estimated numbers of animals needed were derived from our previous experience with

similar experiments and the number of experiments needed to achieve a statistically significant deviation (>20% difference at $p<0.05$) based on a power analysis [96]. The number of biological replicates (*e.g.*, animals, cells, and immunoblot samples) is provided in the corresponding figures and legends. Significances of ICQs of Piezo1 immunocolocalization with NKA and GFAP were analyzed by means of the normal approximation of the nonparametric Wilcoxon rank test, as described previously [41, 95]. Mechanical allodynia and hyperalgesia were compared between groups by unpaired two-tailed Student's *t*-test for vF and Mann-Whitney U test for Pin. The differences of the targeted gene expression by immunoblots and calcium imaging analysis were compared with one-way ANOVA, unpaired two-tailed unpaired *t*-test, or Mann-Whitney U test, where appropriate, as indicated in figure legends. Results are reported as mean and standard deviation of mean (SEM). Differences were considered to be significant for values at $p<0.05$

Results

Specificity of the Piezo1 antibody

IHC on DRG and TG sections from naïve rats (**Fig**. **1A**, **B**) revealed a similar PSN profile of Piezo1 expression, showing higher immunoreactive (IR) density in smaller-sized PSNs. Piezo1 antibody recognized ~300kDa canonical piezo1 band and additional ~220kDa and ~70kDa protein bands upon immunoblot (IB) using DRG lysates from naïve rats (**Fig**. **1C**). Two additional experiments were performed to further validate the specificity of antibody. First, Piezo1 Co-IP followed by IB was performed using rat DRG lysates, which showed that the ~300kDa band but not ~220kDa and ~70kDa protein bands was clearly detected in Piezo1 Co-IP sample. Protein identification by proteomics (liquid chromatography-tandem mass spectrometry, LC-MS/MS) confirmed Piezo1 on the excised band ranging 150~320kDa from the silver stained 1D-PAGE gel of Co-IP samples (**Fig**. **1D-E** and **Suppl**. **Fig**. **1**). Additionally, the keratinocyte Piezo1-IR profile was displayed on IHC of hindpaw skin prepared from wild-type mice (WT), but the Piezo1 immunopositivity was barely detectable in the hindpaw skin prepared from the keratinocyte Piezo1 KO ($K14^{Cre+}/Piezo1^{fl/f}$) mice. The skin Piezo2 staining density in $K14^{Cre+}/Piezo1^{fl/f}$ mice was similar to WT mice, indicating no effect of Piezo1 deletion in skin keratinocytes on Piezo2 expression (**Fig**. **1F-H**). These data provided supporting evidence for Piezo1 antibody used in this study to detect Piezo1 expression by IHC and immunoblots.

Neuronal and glial Piezo1 expression in DRG

We next characterized the Piezo1 expression within DRG sections by double immunolabeling with various established and distinct neuronal markers including Tubb3 (pan neurons),

nonpeptidergic IB4-biotin (nonpeptidergic small neurons), peptidergic CGRP (peptidergic neurons), NKA1α (neuronal plasma membrane), NF200 (large Aβ low-threshold mechanoreceptors, i.e. Aβ-LTMRs and proprioceptors), and Cav3.2 (Aδ- and C-LTMRs) [25]. Results revealed Piezo1-IR in 78% of the Tubb3-positive PSNs (**Fig**. **2A, A1**) with higher IR density in smaller-sized PSNs in rat DRG, a finding that is consistent with the results by RNAscope [83]. All IB4- and CGRP-positive neurons which consist of 33% and 38% of Piezo1-positive neurons, respectively, were Piezo1-IR (**Fig**. **2B, B1, C, C1**), indicating that Piezo1 is expressed by unmyelinated (C-type) and thinly myelinated (Aδ-type) PSNs that convey the thermal and mechanoreceptive nociceptive signals generated at peripheral nerve terminals to neurons in lamina I-II of the spinal cord [20]. Nociceptive neurons in adult rat DRG can be double positive for both IB4 and CGRP (30-40%) [95], suggesting that there is a substantial proportion of small Piezo1-IR neurons positive for both IB4/CGRP. Most (76%) of Piezo1-positive PSNs were also positive for $Ca_V3.2$, suggesting high expression of Piezo1 in the Aδ- and C-LTMR neurons (**Fig**. **2D, D1**) [25]. About 66% of NF200-neurons were Piezo1 immunopositive in a less immunostaining density (**Fig**. **2E, E1**), suggesting detection of Piezo1 expression in the Aβ-LTMRs and proprioceptive PSNs that transmit mechanoreceptive and proprioceptive signals via thickly myelinated afferents to spinal lamina III-V. Colabeling of Piezo1 with NKA1α revealed enriched Piezo1 profiles in the PSN plasma membrane, especially those of larger diameter neurons (**Fig. 2F**). A RNAseq study also reported detection of Piezo1 transcript in mice DRG large neurons expressing neurofilament and parvalbumin, but less enriched than Piezo2 [80]. To obtain further insight into plasma membrane (PM) localization of Piezo1, we examined the ICA of the images co-stained for Piezo1 and NKA1α. Overlaid images of Piezo1 with NKA1α showed colocalizations of the two patterns of immunopositivity (**Fig**.

2F1), but the ICA plots of Piezo1 and NKA1α resulted, however, in a complex relationship in which the data tended to cluster along both positive and negative axes with ICQ 0.04-0.2 (p <0.01~ 0.001, n=10), indicating partial localization of Piezo1 in neuronal PM (**Fig**. **2G**).

Piezo1 has been identified in satellite glial cells in mouse DRG by RNAscope and microarray [6, 32]. Here we performed IHC using various established markers for Schwann cells (SCs) and satellite glial cells (SGCs) which may represent a population of developmentally arrested Schwann cells [27]. Both are composed of perineuronal glia and express glial markers [64] including glutamine synthetase (GS), 3-hydroxy-3-methylglutaryl coenzyme A synthase 1 (Hmgcs1), glial fibrillary acidic protein (GFAP), and S100. IHC staining revealed Piezo1-IR in the GS-, Hmgcs1-, S100-, and GFAP-positive perisomatic glial population (**Fig**. **2H-K**), indicating Piezo1 expression in SGCs and/or SCs since both are composed of perineuronal glia and express those glial markers [64]. To further verify the presence of Piezo1 in the perineuronal glia, ICA was performed to analyze the immunocolocalization between Piezo1 and GFAP. Overlaid images of Piezo1 with GFAP showed colocalizations of two immunopositivity (**Fig**. **2K1**), and the ICA plots of Piezo1 and GFAP also clustered along both positive and negative axes with ICQ 0.06-0.26 (p < 0.01~0.001, n=10), indicating Piezo1 partial colocalization in perineuronal glia cells (**L**). A search of deposited datasets in the GenBank GEO Profile and Human Atlas Protein (https://www.proteinatlas.org) corroborated our finding since Piezo1 transcripts have been detected in the cultured rat and human Schwann cells [22] and SGCs [6, 32]. This provides support for our finding that SGCs and SCs express Piezo1. ICC on rat dissociated DRG culture also identified Piezo1 expression in the somata of neurons and their

neurites, as well as GFAP- and S100-positive glial cells (**Suppl**. **Fig**. **2**). Additionally, neuronal and non-neuronal Piezo1 protein was also detected by IHC in naïve mice DRG (**Suppl**. **Fig**. **3**).

Detection of Piezo1-IR in sciatic nerve, spinal cord, and skin

We next characterized Piezo1 expression in tissues innervated by PSNs. Results showed that Piezo1-IR signals were detected in the tissue sections of sciatic nerve, which co-stained with neuronal markers of IB4, CGRP, Tubb3, and NF200 (**Fig**. **3A-D**), indicating that Piezo1 was actively transported along the peripheral afferent axons. Notably, sciatic nerve Piezo1 was also detected in Schwann cell since Piezo1 signals were colocalized to Schwann cell markers of GFAP, p75NTR, S100, and MBP (**Fig**. **3E-H**). ICC colabeling of Piezo1 with S100 on human SCs and SCs isolated from rat sciatic nerve verified Piezo1 expression in SCs (**Fig**. **3I**, **J**).

Since our IHC findings suggest that Piezo1 is actively transported along the peripheral processes of PSNs (**Fig**. **3**), we examined whether Piezo1 is also transported to the central terminals innervating the spinal cord dorsal horn (DH). Indeed, Piezo1-IR signals were present in the central terminals of peptidergic and nonpeptidergic neuropils that synapse in the DH. These are likely transported along axons from DRG-PSNs since DH Piezo1-IR was highly overlaid to presynaptic markers of IB4, CGRP, synaptic vesicle protein synaptophysin (Syp), and synaptoporin (Synpr) (**Fig**. **4A-D, A1-D1)**, all of which are expressed in small-sized DRG neurons with active axonal transportation [72, 94]. Additionally, we found Piezo1-IR in the intrinsic spinal cord neurons of both the DH and the ventral horn (VH). Colabeling of Piezo1 with NeuN and PKCγ verified Piezo1-IR in the spinal cord neurons, including DH interneurons and VH motor neurons (**Fig**. **4E-G, E1-G1**), in agreement with recent studies that showed

abundant Piezo1 (and Piezo2) transcript in somatostatin interneurons, nociceptive projection neurons of the DH, and ventral horn motor neurons [12, 34, 46, 87]. DH Piezo1-IR was colabeled with GFAP-positive astrocytes (**Fig**. **4H, H1**) and colocalization of Piezo1 and GFAP was verified in spinal DH dissociated glia cultures (**Suppl**. **Fig**. **4**). Finally, Piezo1-IR was also detected in the brain neurons and GFAP-positive astrocytes; and supportively, the functional Piezo1 was verified in the NG108 cortex neuronal cells and brain astrocytes by Yoda1 stimulation (**Suppl**. **Fig**. **5**).

Piezo1 is highly expressed in skin [18], and has been detected in keratinocytes [31, 50] and sensory afferent lanceolate endings [98]. We here characterized Piezo1 protein expression profile in rat hindpaw skin (**Fig**. **5)**. We found Piezo1-IR in the Merkel cells of the hindpaw epidermis, which colabeled with CK14, a marker for the basal keratinocytes and Merkel cells [45, 88]. Images also revealed Piezo1-IR in Meissner's corpuscles, lanceolate endings, onion-shaped Pacinian corpuscle, afferent terminal nerve bundles, and the endothelial cells of small blood vessels within dermis. We also detected the epidermal Syp-IR closely anear Piezo1 keratinocytes, suggestive of Piezo1 keratinocyte–sensory neuron synaptic-like contacts [79], which will require further investigation. S100-IR was overlaid upon the Piezo1-IR signals in cutaneous nerve bundles, Meissner's corpuscles and Schwann cells surrounding cutaneous afferent nerve bundles within dermis, suggesting that Piezo1 was likely expressed by cutaneous Schwann cells. Additionally, Piezo1-IR in the epidermal basal layer keratinocytes was colabeled with S100, which is a well-validated melanocyte (or pigment cells) marker but is absent in Merkel cells [57]. Co-labeling of Piezo1 with S100 by ICC and Yoda1 stimulation on the cultured human epidermal melanocytes verified functional piezo1 expression in the melanocytes (see

below). Together, our data indicate that Piezo1 is abundantly expressed in skin, including the Merkel cells and epidermal melanocytes, various cutaneous sensory corpuscles, sensory terminals, and microvascular networks. Glabrous Meissner's corpuscles were colabeled with Piezo1, NF200, IB4/CGRP, and S100, indicating that the Piezo1-positive Meissner's corpuscles are a multiafferented mechanoreceptor consisting of Aβ and accessories of C/Aδ fibers axons, as well as nonmyelinating SCs [15, 54].

Functional verification of Piezo1 expression in neuronal and nonneuronal cells

Piezo1 is an ion channel that conducts non-selective Ca^{2+} influx into the cytoplasm in various cell types [28] [62, 74]. Piezo1 channels are activated and robustly characterized by mechanical cell indention [18] and high-speed pressure-clamp (HSPC) [9] under the whole cell patch-clamp via heterologous overexpression system and by a heterocyclic compound Yoda1 chemically-stimulated microfluorimetric Ca^{2+} imaging [74]. Because both Piezo1 and Piezo2 co-express in neurons and non-neuronal cells [68, 83], the apparent similarity in Piezo1/2-mediated MA-currents may confound the results of either of Piezo homolog characterization. Although it does not fully mimic mechanical opening dynamics of the channels, Yoda1, a synthetic small molecule agonist capable of selectively activating Piezo1 with micromolar affinity, is a useful research tool to confirm the presence of functional Piezo1 channels and to delineate the functional impact of Piezo1 on various cellular processes and reactions [74]. Selectivity is validated since genetic deletion of Piezo1 by Cas9/CRISPIR system completely abolish Yoda1-induced Ca^{2+} responses [33, 36], Piezo1 knockdown by RNA interference suppresses such effects [85], Yoda1 activates Piezo1 but not Piezo2 consistent with Yoda1 having a Piezo1 selective effect [37, 74], and activation by Yoda1 and by mechanical stimuli are closely coupled

[11, 74]. Moreover, Yoda1 activation on other mechanoreceptors have not been found. Here we tested the ability of Yoda1 to induce Ca^{2+} response in dissociated PSNs, DRG glia (composed of SGCs, SCs, and other non-neuronal populations resident within DRGs), sciatic nerve SCs, and DH glial cells of naïve rats, as well as NSC34 spinal cord motor neuron-like cells, 50B11 DRG neuronal cells, and primary human melanocytes. We observed that Yoda1 induced dose-dependent increases of $[Ca^{2+}]_i$ in all of these cell types (**Fig**. **6**), with apparent variability in magnitude of the $[Ca^{2+}]_i$ response. Sensitivity to Yoda1 stimulation is highest in human epidermal melanocytes, NSC34 cells, followed by rat SCs, isolated DH glial cells, 50B11 cells, and isolated SGCs and DRG neurons (**Fig**. **6** and **suppl**. **Fig**. **6**). Currently, no Piezo1-specific inhibitor is available. Activation of Piezo1 can be sensitively blocked by GsMTx4, which, although antagonizes other MSCs, has been widely used to characterize Piezo1 function stimulated by Yoda1. Results showed that, in all cell types tested, Yoda1 responses were sensitively abolished by the GsMTx4 (0.5~1.0μM). Among rat PSNs, the majority of the responders were small- and medium-sized (**Fig. 6C2**), consistent with a previous report in mice [62] showing that Yoda1 induces inward currents more often in small- and medium-sized PSNs neurons than in large neurons. Even within a neuronal size group, there was substantial variation in the magnitude of $[Ca^{2+}]_i$ response to Yoda1, suggesting functional diversity of Piezo1 in different neuronal subpopulations. Taken together, our study showed that functional Piezo1 is widely expressed in neuronal and non-neuronal cells in peripheral sensory pathways, as well as glial cells in spinal cord of rats.

Increased DRG piezo1 protein levels after painful peripheral nerve injury

Piezo channels are activated after axon injury [70], inflammation promotes Piezo1 activity, and inflammatory signaling sensitizes Piezo1 which can also promote inflammation [39, 69]. We next attempted to determine whether neuropathic pain was associated with alteration of Piezo1 protein levels in rat DRG because neuropathic pain is in a comorbid setting of nerve injury and inflammatory responses. We generated TNI and SNI neuropathic pain, confirmed by reduced the threshold for withdrawal from mild mechanical stimulation (vF) and hyperalgesia evident with noxious (Pin) mechanical stimulation when compared to baseline and sham-operated animals. L4/L5 DRG were harvested at the 28 days after TNI or SNI injury, to evaluate the protein expression level of Piezo1 and microgliosis in the DRG. The canonical Piezo1 (~300KDa) upon immunoblotting was significantly increased in DRG lysates from the DRG ipsilateral to TNI and SNI, comorbid with microgliosis as shown that the Iba1 protein was significantly elevated, compared to controls (**Fig. 7A-D**). We additionally assessed whether TNI-induced neuropathic pain modifies $[Ca^{2+}]_i$ responses to Yoda1 in DRG neurons and SGCs (mix of glia) of adult rats. Functional assessment (application of Yoda1) of the dissociated cultures from DRG ipsilateral to TNI showed that 5 and 10μM of Yoda1-evoked $[Ca^{2+}]_i$ responses were significantly higher in both PSNs (**Fig. 7E-E2**) and SGCs (**Fig 7F-F2**), compared to cells from the sham-operated DRG. Additionally, the responders (%) of both PSNs and SGCs from TNI rats to 10μM Yoda1stimulation were significantly increased, compared to the cells from the sham-operated DRG. These data indicate that both neuronal and non-neuronal Piezo1 were activated following neuropathic pain, potentially contributing to the pain pathogenesis.

Sciatic nerve injection of GsMTx4 attenuates TNI mechanical hypersensitization

Our functional evaluations above indicate that SCs of sciatic nerve are especially sensitive to Yoda1 stimulation. To further investigate whether enhanced Piezo1 in the peripheral sensory nervous system after TNI contributes to pain behavior, we evaluated the effects of ipsilateral sciatic nerve injection of GsMTx4 on mechanical allodynia and hyperalgesia after TNI. Findings from previous studies suggest that intraperitoneal (i.p.) and intradermal application of GsMTx4 is effective in providing analgesia for both inflammatory and neuropathic pain involving MSCs including Piezo1. In this experiment, GsMTx4 effects on mechanical hypersensitization were evaluated 21 days after TNI injury, when peripheral hypersensitivity is fully established [90]. A single delivery of 40 μM GsMTx4 in a volume of 100μL into the sciatic nerve fully reversed pain behaviors 45 min after injection, with return to baseline levels 2 hr after administration (**Fig**. **8A-D**). A smaller dose (100μL, 20 μM) also had an effect, but less complete reversal of pain behaviors. No abnormal ambulation was noted for animals injected with GsMTx4 during the testing period. These data suggest that block of Piezo1 (although inhibition of other pain MSCs) selectively in the peripheral nervous system alleviates mechanical hypersensitivity. This adds further evidence for a possibility that Piezo1 contributes to pain following nerve injury.

Discussion

This report provides affirmative data showing the distribution and the potential roles of Piezo1 in peripheral sensory pathways. First, IHC using a KD/KO validated antibody identifies Piezo1 in most DRG-PSNs (~78%), preferentially in smaller-sized but also in larger-sized neurons, a result likewise to the recent reports by in situ hybridization or calcium imaging showing Piezo1 expression predominantly in the smaller DRG-PSNs but also in some larger PSNs of mice [62, 83]. Secondly, Piezo1 expression in PSNs extends from the peripheral terminals in the skin to the central presynaptic terminals in the spinal DH. Additionally, Piezo1 is expressed by DH neurons, ventral horn motor neurons, astrocytes, and in peripheral non-neuronal cells, including perineuronal glia composed of SGCs and SCs, sciatic nerve and cutaneous SCs, and skin epidermal melanocytes, as well as Merkel cells. Finally, painful nerve injury increases DRG Piezo1 protein levels, which may involve neurons and glial cells since Piezo1 is activated in both PSNs and SGCs following painful neuropathy of rats. These observations suggest that Piezo1 be a mechanotransducer possibly contributing to peripheral nociceptive mechanobiology and pain pathogenesis [83]. Further study is needed to verify Piezo1 MA features related to the functions and pain pathogenesis in these various cells.

Piezo1 was found in the majority of rat PSNs, a similar profile to Piezo2 [68], indicating that both Piezo1/2 co-expression in PSNs, as reported for mice DRG showing >50% of Piezo1-expressing neurons also express Piezo2 [83]. Piezo isoforms are not reported to form Piezo1/2 hybrid, but co-expression of Piezo1/2 in PSNs with apparent similarity in functional properties between Piezo1 and Piezo2 raises the possibility of a functional interaction exists between these channels. Individual expression of either Piezo1 or Piezo2 in the HEK293 cell heterologous

systems is sufficient to induce channel activity, and combined expression of Piezo1/2 by co-transfection potentiates mechanically induced Ca^{2+} signals and MA electrical currents, compared to the expression of single Piezo homolog [38]. This indicates the possibility of Piezo1/2 to cooperate via synergistic interaction. However, PSN-Piezo2^{cKO} mice have impairment of touch but sensitized mechanical sensitivity which is reversed by PSN-Piezo1 knock-in, suggesting a possibility of Piezo1/2 negative interaction [98]. Additionally, *in vitro* knockdown of either of Piezo homologs in Piezo1/2 naturally co-expressing N2A cells significantly decreases mechanically activated (MA) currents [18]. Ablation of Piezo2 selectively in DRG neurons *in vivo* with Piezo1expression intact [68] abolishes MA-currents and reduces mechanical hypersensitivity induced by peripheral nerve injury [51, 75]. Moreover, specific Piezo1 deletion in skin keratinocytes that naturally express both Piezo1/2 induces significant reduction of responses to non-noxious and noxious mechanical stimuli [50]. These observations together imply that Piezo1/2 do not simply serve a redundant or complementary role for each other in mechanotransduction. Because heterologous systems cannot fully mimic *in vivo* conditions of PSNs, it would be interesting to evaluate whether Piezo1 also contributes to pain mechanosensation by PSN-Piezo1^{cKO} and perhaps Piezo1/2 double knockout may be required to further investigate roles of Piezo1/2 in nociceptive mechanosensation other than ablation of either of Piezo isoforms.

The spinal cord DH is a key site for integrating and transmitting somatosensory information [35]. The GenBank GEO Profile and the published literature report detection of Piezo1 (and Piezo2) transcripts in the DH projection neurons, interneurons, and spinal cord motor neurons [12, 34, 46, 87]. Piezo1 is detected in human induced pluripotent stem cell (iPSC)-derived spinal motor

neurons [44], and the Human Protein Atlas shows consensus datasets of Piezo1 transcript sin spinal cord. These data provide credent evidence of Piezo1 in spinal cord transcriptome, and we now confirm Piezo1 protein expression in the spinal cord. Cumulatively, Piezo1 may play unexplored role in spinal cord which organizes descending and ascending mechanosensory and pain signals [40].

Peripheral non-neuronal cells play a key role in the induction and maintenance of persistent mechanical pain [49]. Here, we show that Piezo1 is expressed extensively in the peripheral nerve non-neuronal cells of various types. The skin acts as a complex sensory organ [99], and epidermal keratinocytes along with Merkel cells, Langerhans cells, and melanocytes express sensor proteins that regulate the neurocutaneous system and participate in nociception and mechanotransduction [49]. Non-neuronal skin keratinocytes and the sensory afferent lanceolate endings express Piezo1, which is required for skin mechanotransduction [98]. Our data also reveal Piezo1-IR in Meissner's corpuscles, lanceolate endings, Pacinian corpuscle in deeper dermis, and the afferent terminal nerve bundles. Not only Aβ-LTMR but also C- and Aδ-LTMR fibers innervate lanceolate endings and Meissner's corpuscles that contribute to behavioral responses, perception of light touch, and nociception [2]. Beside detection of Piezo1-IR in the skin epidermal Merkel cells, we also provide evidence that the epidermal melanocytes also express functional Piezo1. Skin melanocytes are dendritic cells, derived from skin Schwann cell precursors that originate from neural crest cells (NCC) and regulate mechanosensation [53]. Melanocytes form tight contacts with cutaneous nerves, respond to mechanical stretch, and appear around nerve fascicles after damage [61]. Pressure-sensing Merkel cells are thought of NCC origin [76], but new observations show that Merkel cells originate from epidermal

progenitors but not NCCs [81]. Moreover, we found that peripheral glia, including SGCs and SCs, express Piezo1, which is colocalized to S100-positive dermal afferent nerve bundles and terminal fibers, indicative of Piezo1 expression in the cutaneous nociceptive SCs.

Sensory neurons and SGCs/SCs, the two principal cell types of the peripheral nerves, interact intimately and are critical for normal peripheral nerve functions and pain pathogenesis during nerve injury and inflammation. Peripheral SCs can sense and transduce mechanical signals involving mechanosensation [8, 63], and the specialized cutaneous nociceptive SCs *in* skin modulate the sensitivity threshold for mechanosensation [1]. New reports indicate that SGCs can promote regenerative growth into PSNs [6] and may even have stem cell characteristics to differentiate to PSNs [82]. SCs in peripheral nerves are critical for both sensory and motor functions. SCs are physiologically exposed to mechanical stresses (i.e., tensile, compressive and shear strains) [8] can sense and transduce mechanical signals involving mechanosensation, and determine the sensitivity threshold for mechanosensation [1, 86]. Therefore, peripheral nerve SCs-Piezo1 may play hitherto unexplored roles in sensory processing and mechanotransduction; for instance, by regulating signaling within SCs initiated by mechanical stimulation. Functional Piezo1 is expressed in mouse and human neural stem cells [19, 56] and both Piezo1/2 express in human embryonic stem cell-derived NCC cells [52, 65]. Thus, it is speculated that Piezos may play roles for mechanosensitive lineage choice and that Piezos expression is required throughout the differentiation process along NCC differentiated sensory neuronal or nonneuronal glial lineages in peripheral nervous system.

The decrease in mechanical hypersensitivity of TNI rats induced by peripheral injection of GsMTx4 adds further evidence for possible involvement of peripheral Piezo1 activation in neuropathic pain. Acute anti-nociception to mechanical stimulation after intraperitoneal and intradermal application of GsMTx4 has been used in addressing possible involvement MSCs including Piezo1 in animal models of chronic pain [3, 55]. Since Piezo1 is also expressed in spinal cords, it is unclear whether peripheral or central block of Piezo1 is analgesia. Analgesic effect by GsMTx4 sciatic injection suggests that a peripheral site of Piezo1 action is possibly involved in pain generation. GsMTx4 directly into the large nerve trunks of the sciatic nerve could act on axonal Piezo1channels directly at the site of injection, or may spread to more central and peripheral sites of action by bulk flow and diffusion longitudinally within the sciatic and associated spinal nerves, or by axoplasmic transport. Additionally, the effects could attribute to block of sciatic nerve SCs-Piezo1, since Piezo1 is also abundantly expressed by SCs. The observed GsMTx4 analgesia is, at least in part, due to inhibition on Piezo1, although alternative targets are possible since GsMTx4 inhibits several nociceptive molecules, such as Trpv4, Trpa1, Trpc1/6 and TACAN [3, 7]. TRP channels but not TACAN is reported to contribute neuropathic hyperalgesia in rats and Piezo1 activation may trigger TRP channels, e.g., Trpv4 [3, 10, 73]. A genetic approach of conditional ablation of Piezo1 in peripheral neurons or specific glial cells in future study will help to elucidate the role of Piezo1 in peripheral mechanobiology and in pain pathogenesis. Finally, sciatic nerves at the midthigh are composed of axonal fibers from sensory, motor, and sympathetic neurons that may also express Piezo1 and other MSCs; thus, the analgesic effect may be partially resulted from Piezo1 inhibition in those fibers and wrapped SCs that may also play roles in generation of pain behavior.

References

[1] Abdo H, Calvo-Enrique L, Lopez JM, Song J, Zhang MD, Usoskin D, El Manira A, Adameyko I, Hjerling-Leffler J, Ernfors P. Specialized cutaneous Schwann cells initiate pain sensation. Science 2019;365(6454):695-699.

[2] Abraira VE, Ginty DD. The sensory neurons of touch. Neuron 2013;79(4):618-639.

[3] Alessandri-Haber N, Dina OA, Chen X, Levine JD. TRPC1 and TRPC6 channels cooperate with TRPV4 to mediate mechanical hyperalgesia and nociceptor sensitization. J Neurosci 2009;29(19):6217-6228.

[4] Alper SL. Genetic Diseases of PIEZO1 and PIEZO2 Dysfunction. Curr Top Membr 2017;79:97-134.

[5] Andersen ND, Srinivas S, Pinero G, Monje PV. A rapid and versatile method for the isolation, purification and cryogenic storage of Schwann cells from adult rodent nerves. Sci Rep 2016;6:31781.

[6] Avraham O, Deng PY, Jones S, Kuruvilla R, Semenkovich CF, Klyachko VA, Cavalli V. Satellite glial cells promote regenerative growth in sensory neurons. Nat Commun 2020;11(1):4891.

[7] Beaulieu-Laroche L, Christin M, Donoghue A, Agosti F, Yousefpour N, Petitjean H, Davidova A, Stanton C, Khan U, Dietz C, Faure E, Fatima T, MacPherson A, Mouchbahani-Constance S, Bisson DG, Haglund L, Ouellet JA, Stone LS, Samson J, Smith MJ, Ask K, Ribeiro-da-Silva A, Blunck R, Poole K, Bourinet E, Sharif-Naeini R. TACAN Is an Ion Channel Involved in Sensing Mechanical Pain. Cell 2020;180(5):956-967 e917.

[8] Belin S, Zuloaga KL, Poitelon Y. Influence of Mechanical Stimuli on Schwann Cell Biology. Front Cell Neurosci 2017;11:347.

[9] Besch SR, Suchyna T, Sachs F. High-speed pressure clamp. Pflugers Arch 2002;445(1):161-166.

[10] Bonet IJM, Araldi D, Bogen O, Levine JD. Involvement of TACAN, a Mechanotransducing Ion Channel, in Inflammatory But Not Neuropathic Hyperalgesia in the Rat. J Pain 2021;22(5):498-508.

[11] Botello-Smith WM, Jiang W, Zhang H, Ozkan AD, Lin YC, Pham CN, Lacroix JJ, Luo Y. A mechanism for the activation of the mechanosensitive Piezo1 channel by the small molecule Yoda1. Nat Commun 2019;10(1):4503.

[12] Chamessian A, Young M, Qadri Y, Berta T, Ji RR, Van de Ven T. Transcriptional Profiling of Somatostatin Interneurons in the Spinal Dorsal Horn. Sci Rep 2018;8(1):6809.

[13] Chen X, Wanggou S, Bodalia A, Zhu M, Dong W, Fan JJ, Yin WC, Min HK, Hu M, Draghici D, Dou W, Li F, Coutinho FJ, Whetstone H, Kushida MM, Dirks PB, Song Y, Hui

CC, Sun Y, Wang LY, Li X, Huang X. A Feedforward Mechanism Mediated by Mechanosensitive Ion Channel PIEZO1 and Tissue Mechanics Promotes Glioma Aggression. Neuron 2018;100(4):799-815 e797.

[14] Chesler AT, Szczot M, Bharucha-Goebel D, Ceko M, Donkervoort S, Laubacher C, Hayes LH, Alter K, Zampieri C, Stanley C, Innes AM, Mah JK, Grosmann CM, Bradley N, Nguyen D, Foley AR, Le Pichon CE, Bonnemann CG. The Role of PIEZO2 in Human Mechanosensation. N Engl J Med 2016;375(14):1355-1364.

[15] Cobo R, Garcia-Piqueras J, Cobo J, Vega JA. The Human Cutaneous Sensory Corpuscles: An Update. J Clin Med 2021;10(2):227.

[16] Copp SW, Kim JS, Ruiz-Velasco V, Kaufman MP. The mechano-gated channel inhibitor GsMTx4 reduces the exercise pressor reflex in decerebrate rats. J Physiol 2016;594(3):641-655.

[17] Copp SW, Kim JS, Ruiz-Velasco V, Kaufman MP. The mechano-gated channel inhibitor GsMTx4 reduces the exercise pressor reflex in rats with ligated femoral arteries. Am J Physiol Heart Circ Physiol 2016;310(9):H1233-1241.

[18] Coste B, Mathur J, Schmidt M, Earley TJ, Ranade S, Petrus MJ, Dubin AE, Patapoutian A. Piezo1 and Piezo2 are essential components of distinct mechanically activated cation channels. Science 2010;330(6000):55-60.

[19] Del Marmol JI, Touhara KK, Croft G, MacKinnon R. Piezo1 forms a slowly-inactivating mechanosensory channel in mouse embryonic stem cells. Elife 2018;7:33149.33001.

[20] Dubin AE, Patapoutian A. Nociceptors: the sensors of the pain pathway. J Clin Invest 2010;120(11):3760-3772.

[21] Duncan C, Mueller S, Simon E, Renger JJ, Uebele VN, Hogan QH, Wu HE. Painful nerve injury decreases sarco-endoplasmic reticulum Ca(2)(+)-ATPase activity in axotomized sensory neurons. Neuroscience 2013;231:247-257.

[22] El Soury M, Fornasari BE, Morano M, Grazio E, Ronchi G, Incarnato D, Giacobini M, Geuna S, Provero P, Gambarotta G. Soluble Neuregulin1 Down-Regulates Myelination Genes in Schwann Cells. Front Mol Neurosci 2018;11:157.

[23] Fischer G, Kostic S, Nakai H, Park F, Sapunar D, Yu H, Hogan Q. Direct injection into the dorsal root ganglion: technical, behavioral, and histological observations. J Neurosci Methods 2011;199(1):43-55.

[24] Flegel C, Schobel N, Altmuller J, Becker C, Tannapfel A, Hatt H, Gisselmann G. RNA-Seq Analysis of Human Trigeminal and Dorsal Root Ganglia with a Focus on Chemoreceptors. PLoS One 2015;10(6):e0128951.

[25] Francois A, Schuetter N, Laffray S, Sanguesa J, Pizzoccaro A, Dubel S, Mantilleri A, Nargeot J, Noel J, Wood JN, Moqrich A, Pongs O, Bourinet E. The Low-Threshold Calcium

Channel Cav3.2 Determines Low-Threshold Mechanoreceptor Function. Cell Rep 2015;10(3):370-382.

[26] Gemes G, Bangaru ML, Wu HE, Tang Q, Weihrauch D, Koopmeiners AS, Cruikshank JM, Kwok WM, Hogan QH. Store-operated Ca2+ entry in sensory neurons: functional role and the effect of painful nerve injury. J Neurosci 2011;31(10):3536-3549.

[27] George D, Ahrens P, Lambert S. Satellite glial cells represent a population of developmentally arrested Schwann cells. Glia 2018;66(7):1496-1506.

[28] Glogowska E, Schneider ER, Maksimova Y, Schulz VP, Lezon-Geyda K, Wu J, Radhakrishnan K, Keel SB, Mahoney D, Freidmann AM, Altura RA, Gracheva EO, Bagriantsev SN, Kalfa TA, Gallagher PG. Novel mechanisms of PIEZO1 dysfunction in hereditary xerocytosis. Blood 2017;130(16):1845-1856.

[29] Gonzalez S, Fernando RN, Perrin-Tricaud C, Tricaud N. In vivo introduction of transgenes into mouse sciatic nerve cells in situ using viral vectors. Nat Protoc 2014;9(5):1160-1169.

[30] He BH, Christin M, Mouchbahani-Constance S, Davidova A, Sharif-Naeini R. Mechanosensitive ion channels in articular nociceptors drive mechanical allodynia in osteoarthritis. Osteoarthritis Cartilage 2017;25(12):2091-2099.

[31] Holt J, Zeng W, Evens E, Woo S, Ma S, Abuwarda H, Loud M, Loud M, Patapoutian A, Pathak MM. Spatiotemporal dynamics of PIEZO1 localization controls keratinocyte migration during wound healing
. 2000, bioRvix doi: https://doiorg/101101/20201018344598.

[32] Jager SE, Pallesen LT, Richner M, Harley P, Hore Z, McMahon S, Denk F, Vaegter CB. Changes in the transcriptional fingerprint of satellite glial cells following peripheral nerve injury. Glia 2020;68(7):1375-1395.

[33] Jiang F, Yin K, Wu K, Zhang M, Wang S, Cheng H, Zhou Z, Xiao B. The mechanosensitive Piezo1 channel mediates heart mechano-chemo transduction. Nat Commun 2021;12(1):869.

[34] Kaplan A, Spiller KJ, Towne C, Kanning KC, Choe GT, Geber A, Akay T, Aebischer P, Henderson CE. Neuronal matrix metalloproteinase-9 is a determinant of selective neurodegeneration. Neuron 2014;81(2):333-348.

[35] Koch SC, Acton D, Goulding M. Spinal Circuits for Touch, Pain, and Itch. Annu Rev Physiol 2018;80:189-217.

[36] Kuriyama k, Hirose H, Masuda T, Shudou M, Arafiles JVV, Imanishi M, Yuji Hara MM, Futaki S. Piezo1 activation using Yoda1 inhibits macropinocytosis and proliferation of cancer cells. bioRxiv 2021 doi: https://doiorg/101101/20210514444123 2021.

[37] Lacroix JJ, Botello-Smith WM, Luo Y. Probing the gating mechanism of the mechanosensitive channel Piezo1 with the small molecule Yoda1. Nat Commun 2018;9(1):2029.

[38] Lee W, Leddy HA, Chen Y, Lee SH, Zelenski NA, McNulty AL, Wu J, Beicker KN, Coles J, Zauscher S, Grandl J, Sachs F, Guilak F, Liedtke WB. Synergy between Piezo1 and Piezo2 channels confers high-strain mechanosensitivity to articular cartilage. Proc Natl Acad Sci U S A 2014;111(47):E5114-5122.

[39] Lee W, Nims RJ, Savadipour A, Zhang Q, Leddy HA, Liu F, McNulty AL, Chen Y, Guilak F, Liedtke WB. Inflammatory signaling sensitizes Piezo1 mechanotransduction in articular chondrocytes as a pathogenic feed-forward mechanism in osteoarthritis. Proc Natl Acad Sci U S A 2021;118(13):e2001611118.

[40] Li L, Rutlin M, Abraira VE, Cassidy C, Kus L, Gong S, Jankowski MP, Luo W, Heintz N, Koerber HR, Woodbury CJ, Ginty DD. The functional organization of cutaneous low-threshold mechanosensory neurons. Cell 2011;147(7):1615-1627.

[41] Li Q, Lau A, Morris TJ, Guo L, Fordyce CB, Stanley EF. A syntaxin 1, Galpha(o), and N-type calcium channel complex at a presynaptic nerve terminal: analysis by quantitative immunocolocalization. J Neurosci 2004;24(16):4070-4081.

[42] Liu Q, Sun B, Zhao J, Wang Q, An F, Hu X, Yang Z, Xu J, Tan M, Li L. Increased Piezo1 channel activity in interstitial Cajal-like cells induces bladder hyperactivity by functionally interacting with NCX1 in rats with cyclophosphamide-induced cystitis. Exp Mol Med 2018;50(5):1-16.

[43] Lopes DM, Denk F, McMahon SB. The Molecular Fingerprint of Dorsal Root and Trigeminal Ganglion Neurons. Front Mol Neurosci 2017;10:304.

[44] Maciel R, Bis DM, Rebelo AP, Saghira C, Zuchner S, Saporta MA. The human motor neuron axonal transcriptome is enriched for transcripts related to mitochondrial function and microtubule-based axonal transport. Exp Neurol 2018;307:155-163.

[45] Maksimovic S, Nakatani M, Baba Y, Nelson AM, Marshall KL, Wellnitz SA, Firozi P, Woo SH, Ranade S, Patapoutian A, Lumpkin EA. Epidermal Merkel cells are mechanosensory cells that tune mammalian touch receptors. Nature 2014;509(7502):617-621.

[46] Marques RF, Engler JB, Kuchler K, Jones RA, Lingner T, Salinas G, Gillingwater TH, Friese MA, Duncan KE. Motor neuron translatome reveals deregulation of SYNGR4 and PLEKHB1 in mutant TDP-43 amyotrophic lateral sclerosis models. Hum Mol Genet 2020;29(16):2647-2661.

[47] Mikhailov N, Leskinen J, Fagerlund I, Poguzhelskaya E, Giniatullina R, Gafurov O, Malm T, Karjalainen T, Grohn O, Giniatullin R. Mechanosensitive meningeal nociception via Piezo channels: Implications for pulsatile pain in migraine? Neuropharmacology 2019;149:113-123.

[48] Moayeri N, Groen GJ. Differences in quantitative architecture of sciatic nerve may explain differences in potential vulnerability to nerve injury, onset time, and minimum effective anesthetic volume. Anesthesiology 2009;111(5):1128-1134.

[49] Moehring F, Halder P, Seal RP, Stucky CL. Uncovering the Cells and Circuits of Touch in Normal and Pathological Settings. Neuron 2018;100(2):349-360.

[50] Moehring F, Mikesell AR, Sadler KE, Menzel AD, Stucky CL. Piezo1 Mediates Keratinocyte Mechanotransduction. bioRvix 2020; doi: https://doiorg/101101/20200719211086 .

[51] Murthy SE, Loud MC, Daou I, Marshall KL, Schwaller F, Kuhnemund J, Francisco AG, Keenan WT, Dubin AE, Lewin GR, Patapoutian A. The mechanosensitive ion channel Piezo2 mediates sensitivity to mechanical pain in mice. Sci Transl Med 2018;10(462).

[52] Nickolls AR, Lee MM, Espinoza DF, Szczot M, Lam RM, Wang Q, Beers J, Zou J, Nguyen MQ, Solinski HJ, AlJanahi AA, Johnson KR, Ward ME, Chesler AT, Bonnemann CG. Transcriptional Programming of Human Mechanosensory Neuron Subtypes from Pluripotent Stem Cells. Cell Rep 2020;30(3):932-946 e937.

[53] Ono K, Viet CT, Ye Y, Dang D, Hitomi S, Toyono T, Inenaga K, Dolan JC, Schmidt BL. Cutaneous pigmentation modulates skin sensitivity via tyrosinase-dependent dopaminergic signalling. Sci Rep 2017;7(1):9181.

[54] Pare M, Elde R, Mazurkiewicz JE, Smith AM, Rice FL. The Meissner corpuscle revised: a multiafferented mechanoreceptor with nociceptor immunochemical properties. J Neurosci 2001;21(18):7236-7246.

[55] Park SP, Kim BM, Koo JY, Cho H, Lee CH, Kim M, Na HS, Oh U. A tarantula spider toxin, GsMTx4, reduces mechanical and neuropathic pain. Pain 2008;137(1):208-217.

[56] Pathak MM, Nourse JL, Tran T, Hwe J, Arulmoli J, Le DT, Bernardis E, Flanagan LA, Tombola F. Stretch-activated ion channel Piezo1 directs lineage choice in human neural stem cells. Proc Natl Acad Sci U S A 2014;111(45):16148-16153.

[57] Petersson S, Shubbar E, Enerback L, Enerback C. Expression patterns of S100 proteins in melanocytes and melanocytic lesions. Melanoma Res 2009;19(4):215-225.

[58] Ranade SS, Qiu Z, Woo SH, Hur SS, Murthy SE, Cahalan SM, Xu J, Mathur J, Bandell M, Coste B, Li YS, Chien S, Patapoutian A. Piezo1, a mechanically activated ion channel, is required for vascular development in mice. Proc Natl Acad Sci U S A 2014;111(28):10347-10352.

[59] Ranade SS, Syeda R, Patapoutian A. Mechanically Activated Ion Channels. Neuron 2015;87(6):1162-1179.

[60] Ranade SS, Woo SH, Dubin AE, Moshourab RA, Wetzel C, Petrus M, Mathur J, Begay V, Coste B, Mainquist J, Wilson AJ, Francisco AG, Reddy K, Qiu Z, Wood JN, Lewin GR, Patapoutian A. Piezo2 is the major transducer of mechanical forces for touch sensation in mice. Nature 2014;516(7529):121-125.

[61] Rizvi TA, Huang Y, Sidani A, Atit R, Largaespada DA, Boissy RE, Ratner N. A novel cytokine pathway suppresses glial cell melanogenesis after injury to adult nerve. J Neurosci 2002;22(22):9831-9840.

[62] Roh J, Hwang SM, Lee SH, Lee K, Kim YH, Park CK. Functional Expression of Piezo1 in Dorsal Root Ganglion (DRG) Neurons. Int J Mol Sci 2020;21(11):3834.

[63] Rosso G, Young P, Shahin V. Implications of Schwann Cells Biomechanics and Mechanosensitivity for Peripheral Nervous System Physiology and Pathophysiology. Front Mol Neurosci 2017;10:345.

[64] Saitoh F, Araki T. Proteasomal degradation of glutamine synthetase regulates schwann cell differentiation. J Neurosci 2010;30(4):1204-1212.

[65] Schrenk-Siemens K, Wende H, Prato V, Song K, Rostock C, Loewer A, Utikal J, Lewin GR, Lechner SG, Siemens J. PIEZO2 is required for mechanotransduction in human stem cell-derived touch receptors. Nat Neurosci 2015;18(1):10-16.

[66] Shin SM, Cai Y, Itson-Zoske B, Qiu C, Hao X, Xiang H, Hogan QH, Yu H. Enhanced T-type calcium channel 3.2 activity in sensory neurons contributes to neuropathic-like pain of monosodium iodoacetate-induced knee osteoarthritis. Mol Pain 2020;16:1744806920963807.

[67] Shin SM, Itson-Zoske B, Cai Y, Qiu C, Pan B, Stucky CL, Hogan QH, Yu H. Satellite glial cells in sensory ganglia express functional transient receptor potential ankyrin 1 that is sensitized in neuropathic and inflammatory pain. Mol Pain 2020;16:1744806920925425.

[68] Shin SM, Moehring F, Itson-Zoske B, Fan F, Stucky CL, Hogan QH, Yu H. Piezo2 mechanosensitive ion channel is located to sensory neurons and nonneuronal cells in rat peripheral sensory pathway: implications in pain. PAIN 2021;Jun 17. doi: 10.1097/j.pain.0000000000002356. Epub ahead of print. PMID: 34285153.

[69] Solis AG, Bielecki P, Steach HR, Sharma L, Harman CCD, Yun S, de Zoete MR, Warnock JN, To SDF, York AG, Mack M, Schwartz MA, Dela Cruz CS, Palm NW, Jackson R, Flavell RA. Mechanosensation of cyclical force by PIEZO1 is essential for innate immunity. Nature 2019;573(7772):69-74.

[70] Song Y, Li D, Farrelly O, Miles L, Li F, Kim SE, Lo TY, Wang F, Li T, Thompson-Peer KL, Gong J, Murthy SE, Coste B, Yakubovich N, Patapoutian A, Xiang Y, Rompolas P, Jan LY, Jan YN. The Mechanosensitive Ion Channel Piezo Inhibits Axon Regeneration. Neuron 2019;102(2):373-389 e376.

[71] Sugisawa E, Takayama Y, Takemura N, Kondo T, Hatakeyama S, Kumagai Y, Sunagawa M, Tominaga M, Maruyama K. RNA Sensing by Gut Piezo1 Is Essential for Systemic Serotonin Synthesis. Cell 2020;182(3):609-624 e621.

[72] Sun T, Xiao HS, Zhou PB, Lu YJ, Bao L, Zhang X. Differential expression of synaptoporin and synaptophysin in primary sensory neurons and up-regulation of synaptoporin after peripheral nerve injury. Neuroscience 2006;141(3):1233-1245.

[73] Swain SM, Romac JM, Shahid RA, Pandol SJ, Liedtke W, Vigna SR, Liddle RA. TRPV4 channel opening mediates pressure-induced pancreatitis initiated by Piezo1 activation. J Clin Invest 2020;130(5):2527-2541.

[74] Syeda R, Xu J, Dubin AE, Coste B, Mathur J, Huynh T, Matzen J, Lao J, Tully DC, Engels IH, Petrassi HM, Schumacher AM, Montal M, Bandell M, Patapoutian A. Chemical activation of the mechanotransduction channel Piezo1. Elife 2015;4:07369.07001.

[75] Szczot M, Liljencrantz J, Ghitani N, Barik A, Lam R, Thompson JH, Bharucha-Goebel D, Saade D, Necaise A, Donkervoort S, Foley AR, Gordon T, Case L, Bushnell MC, Bonnemann CG, Chesler AT. PIEZO2 mediates injury-induced tactile pain in mice and humans. Sci Transl Med 2018;10(462).

[76] Szeder V, Grim M, Halata Z, Sieber-Blum M. Neural crest origin of mammalian Merkel cells. Dev Biol 2003;253(2):258-263.

[77] Talagas M, Lebonvallet N, Berthod F, Misery L. Cutaneous nociception: Role of keratinocytes. Exp Dermatol 2019;28(12):1466-1469.

[78] Talagas M, Lebonvallet N, Berthod F, Misery L. Lifting the veil on the keratinocyte contribution to cutaneous nociception. Protein Cell 2020;11(4):239-250.

[79] Talagas M, Lebonvallet N, Leschiera R, Sinquin G, Elies P, Haftek M, Pennec JP, Ressnikoff D, La Padula V, Le Garrec R, L'Herondelle K, Mignen O, Le Pottier L, Kerfant N, Reux A, Marcorelles P, Misery L. Keratinocytes Communicate with Sensory Neurons via Synaptic-like Contacts. Ann Neurol 2020;88(6):1205-1219.

[80] Usoskin D, Furlan A, Islam S, Abdo H, Lonnerberg P, Lou D, Hjerling-Leffler J, Haeggstrom J, Kharchenko O, Kharchenko PV, Linnarsson S, Ernfors P. Unbiased classification of sensory neuron types by large-scale single-cell RNA sequencing. Nat Neurosci 2015;18(1):145-153.

[81] Van Keymeulen A, Mascre G, Youseff KK, Harel I, Michaux C, De Geest N, Szpalski C, Achouri Y, Bloch W, Hassan BA, Blanpain C. Epidermal progenitors give rise to Merkel cells during embryonic development and adult homeostasis. J Cell Biol 2009;187(1):91-100.

[82] Wang D, Lu J, Xu X, Yuan Y, Zhang Y, Xu J, Chen H, Liu J, Shen Y, Zhang H. Satellite Glial Cells Give Rise to Nociceptive Sensory Neurons. Stem Cell Rev Rep 2021;17(3):999-1013.

[83] Wang J, La JH, Hamill OP. PIEZO1 Is Selectively Expressed in Small Diameter Mouse DRG Neurons Distinct From Neurons Strongly Expressing TRPV1. Front Mol Neurosci 2019;12:178.

[84] Wang S, Cao S, Arhatte M, Li D, Shi Y, Kurz S, Hu J, Wang L, Shao J, Atzberger A, Wang Z, Wang C, Zang W, Fleming I, Wettschureck N, Honore E, Offermanns S. Adipocyte Piezo1 mediates obesogenic adipogenesis through the FGF1/FGFR1 signaling pathway in mice. Nat Commun 2020;11(1):2303.

[85] Wang S, Chennupati R, Kaur H, Iring A, Wettschureck N, Offermanns S. Endothelial cation channel PIEZO1 controls blood pressure by mediating flow-induced ATP release. J Clin Invest 2016;126(12):4527-4536.

[86] Wei Z, Fei Y, Su W, Chen G. Emerging Role of Schwann Cells in Neuropathic Pain: Receptors, Glial Mediators and Myelination. Front Cell Neurosci 2019;13:116.

[87] Wercberger R, Braz JM, Weinrich JA, Basbaum AI. Pain and itch processing by subpopulations of molecularly diverse spinal and trigeminal projection neurons. Proc Natl Acad Sci U S A 2021;118(28).

[88] Woo SH, Ranade S, Weyer AD, Dubin AE, Baba Y, Qiu Z, Petrus M, Miyamoto T, Reddy K, Lumpkin EA, Stucky CL, Patapoutian A. Piezo2 is required for Merkel-cell mechanotransduction. Nature 2014;509(7502):622-626.

[89] Wu HE, Gemes G, Zoga V, Kawano T, Hogan QH. Learned avoidance from noxious mechanical simulation but not threshold semmes weinstein filament stimulation after nerve injury in rats. J Pain 2010;11(3):280-286.

[90] Xiang H, Liu Z, Wang F, Xu H, Roberts C, Fischer G, Stucky C, Caron D, Pan B, Hogan Q, Yu H. Primary sensory neuron-specific interference of TRPV1 signaling by AAV-encoded TRPV1 peptide aptamer attenuates neuropathic pain. Mol Pain 2017;13:1744806917717040.

[91] Xiao B. Levering Mechanically Activated Piezo Channels for Potential Pharmacological Intervention. Annu Rev Pharmacol Toxicol 2020;60:195-218.

[92] Yu H, Fischer G, Ferhatovic L, Fan F, Light AR, Weihrauch D, Sapunar D, Nakai H, Park F, Hogan QH. Intraganglionic AAV6 results in efficient and long-term gene transfer to peripheral sensory nervous system in adult rats. PLoS One 2013;8(4):e61266.

[93] Yu H, Fischer G, Jia G, Reiser J, Park F, Hogan QH. Lentiviral gene transfer into the dorsal root ganglion of adult rats. Mol Pain 2011;7:63.

[94] Yu H, Pan B, Weyer A, Wu HE, Meng J, Fischer G, Vilceanu D, Light AR, Stucky C, Rice FL, Hudmon A, Hogan Q. CaMKII Controls Whether Touch Is Painful. J Neurosci 2015;35(42):14086-14102.

[95] Yu H, Shin SM, Wang F, Xu H, Xiang H, Cai Y, Itson-Zoske B, Hogan QH. Transmembrane protein 100 is expressed in neurons and glia of dorsal root ganglia and is reduced after painful nerve injury. Pain Rep 2019;4(1):e703.

[96] Yu H, Shin SM, Xiang H, Chao D, Cai Y, Xu H, Khanna R, Pan B, Hogan QH. AAV-encoded CaV2.2 peptide aptamer CBD3A6K for primary sensory neuron-targeted treatment of established neuropathic pain. Gene Ther 2019;26(7-8):308-323.

[97] Yu H, Wakim B, Li M, Halligan B, Tint GS, Patel SB. Quantifying raft proteins in neonatal mouse brain by 'tube-gel' protein digestion label-free shotgun proteomics. Proteome Sci 2007;5:17.

[98] Zhang M, Wang Y, Geng J, Zhou S, Xiao B. Mechanically Activated Piezo Channels Mediate Touch and Suppress Acute Mechanical Pain Response in Mice. Cell Rep 2019;26(6):1419-1431 e1414.

[99] Zimmerman A, Bai L, Ginty DD. The gentle touch receptors of mammalian skin. Science 2014;346(6212):950-954.

Legend

Figure 1. Specificity of Piezo1 (PZ1) antibody. Representative IHC images show PZ1-IR (red) preferably in the smaller-sized PSNs in the sections of DRG (**A**) and TG (**B**) from adult naïve rats. Canonical PZ1 at the mass size of ~300 is detected upon immunoblot (IB) of the DRG lysates, with additional protein bands at ~200 and ~70 KDa (**C**). These protein bands are detected in the reduced total lysate proteins loaded on the gel (**D**, left size) but only canonical PZ1 is clearly detected in Piezo1 Co-IP samples (**D**, right size, asterisk denotes IgG heavy chain). Co-IP samples was size-separated, silver stained (**E,** asterisk denotes IgG heavy chain), and gel pieces ranging ~320-150kDa excised in which the rat PZ1 was identified upon mass spectrometry (see **Suppl. Fig. 1**). Representative IHC montage images of colabeling of Piezo1 (PZ1 or Piezo2, red) with CK14 (green) on FFPE sections of hindpaw skin from wide-type (WT) mice (**F**) and Piezo1-ko mice (**G, H**), as indicated. Scale bars: 50μm for A, B; 25μm for F-H.

Figure 2. DRG Piezo1 (PZ1): Double immunostaining. Representative montage images of DRG sections show Piezo1-IR (red) co-stained with PSN markers (green), including Tubb3 (**A**), CGRP (**B**), IB4 (**C**), Cav3.2 (**D**), NF200 (**E**), and NKA1α (**F**, **F1**). The panels in the right-side of **A**-**E** calculate the percentage of Piezo1-neurons overlaid to Tubb3-neurons (**A**1), neurons positive for CGRP/PZ1 (**B1**) and IB4/PZ1 (**C1**) overlaid to PZ1-neurons, and PZ1-neurons overlaid to Cav3.2 (**D1**) and NF200 (**E1**) neurons. The numbers are the counted Piezo1-IR neurons (red) and marker-labeled neurons (green). ICA analyzes colocalization between PZ1 and NKA1α and scatter plots for the region demarcated by the white dashed line in panel **F1** show data clustered along both positive and negative axes for both Piezo1 and NKA1α (**G**). "A" is the

intensity of Piezo1 while "a" is the average of these values, and "B" is the intensity of NKA1a while "b" is the average of these values. For this region, the ICQ value is 0.059 ($P_{sign\ test}$<0.001). (**H-L**) show Piezo1 (red) with a selection of glial cell markers (green), including GS (**H**), Hmgcs1 (**I**) with the squared region shown at high magnification (**I1**), S100 (**J**) with the squared region shown at high magnification (**J1**), and GFAP (**K, K1**). White arrowheads in panel **I1**, **J1**, point to the colabeled glial cells. ICA analysis for colocalization between Piezo1 and GFAP for the region demarcated by the white dashed line in panel **K1** show scattered plot data clustered along both positive and negative axes for both Piezo1 and GFAP (**L**). "A" is the intensity of Piezo1 while "a" is the average of these values, and "B" is the intensity of GFAP while "b" is the average of these values. For this region, the intensity correlation quotient (ICQ) value is 0.122 ($P_{sign\ test}$<0.001). Scale bars: 50μm for all.

Figure 3. IHC delineation of Piezo1 (PZ1) axonal component and Schwann cell expression. Shown are representative IHC montage images on sciatic nerve sections. Double immunostaining of Piezo1 (red) with a selection of neuronal markers (green), including Ib4 (**A**), CGRP (**B**), Tubb3 (**C**), and NF200 (**D**); and Piezo1 (red) with glia markers (green), including GFAP (**E**), p75NTR (**F**), S100 (**G**), and MBP (**H**). Human Schwann cells (**I**) and isolated Schwann cells (**J**) from rat sciatic nerve show double staining of Piezo1 (red) with S100 (green). Scale bars: 50μm for all.

Figure 4. IHC delineation of Piezo1 (PZ1) expression in spinal cord. Shown are representative montage images of double immunostaining on the DH sections of rats. Results reveal Piezo1-IR (red) with a selection of dorsal horn presynaptic markers (green), including IB4

(**A**), CGRP (**B**), Syp (**C**), and Synpr (**D**), showing immunocolocalization (yellow) in the magnified merged images (**A**1-**C**1). **D1** is the squared region of panel **D**. Piezo1-IR (red) and NeuN (green) on the DH (**E**) and ventral horn (**F**) show immunocolocalization (yellow) of PZ1 with the squared region of panel **E** showing the magnified image (**E**1) and amplified image showing PZ1-labeled VH neurons (**F1**). Piezo1-IR (red) and PKCγ (green) on the DH (**G**) show immunocolocalization (yellow) in the magnified merged images (**G**1). Representative montage images (**H)** show positive PZ1 in GFAP-positive astrocytes on spinal cord DH sections, with the squared region shown at high magnification (**H**1). Scale bars: 50μm for all.

Figure 5. IHC delineation of Piezo1 (PZ1) expression in skin. Shown are the representative IHC montage images of immunostaining of PZ1 with different markers on the skin sections (**A**-**T**) and ICC on cultural human melanocytes (**U**-**Y**). Hindpaw glabrous skin sections display PZ1 (red) and CK14 (green), showing colabeling (yellow, empty arrowheads) in the merged image (**A, B**); the white arrowheads point to PZ-1 labeled Meissner corpuscles. PZ1-IR in Meissner's corpuscles (white arrowheads) is immunolocalized with NF200 (**C**), IB4 (**D**), and CGRP) (**E**). PZ1-IR in the hairy skin lanceolate endings is colabeled with NF200 (**F**, white arrowheads) and CGRP around hair follicles (**G**, white arrowheads point to lanceolate endings), as well as putative onion-like Pacinian corpuscle colabeled with NF200 (**H**). PA1-IR is immunocolocalized with CGRP (**I**) and IB4 (**J**), NF200 (**K**), Cav3.2 (**L**), and S100 (**M**) in the nerve bundles within dermis. IHC reveals colabeling of PZ1 (red) with Syn (green) in the nerve bundles within the dermis (**N**, white arrowheads; red arrowheads point to PZ1-labeled endothelial cells of small vesicles). PZ1 (red) is colabeled with Syn (green) in the epidermis (**O**), with the squared region rotated clockwise 90-degree shown at high magnification (**O1**). PZ1 (red) is co-stained with

ACTA2 (green) in the nerve bundles within the dermis (**P**, arrowheads point to nerve bundles (white), to PZ1-labeled endothelial cells of small vesicles (red), and to ACTA2-labled vascular smooth muscles (green). IHC shows PZ1-IR colabeled with S100 in Meissner's corpuscles (white arrowheads) (**Q, R**), with the squared region in panel Q shown at high magnification (**Q1**); and in epidermal basal layer cells (**S** and **T**, empty arrowheads; white arrowheads point to Meissner corpuscles). Human melanocytes (**U**) show Piezo1-IR (**V**) which is completely eliminated by blocking peptide preabsorption before ICC (**W**) and colabeled with S100 (**X**). Scale bars: 25μm for all.

Figure 6. Yoda1-stimualted functional Piezo1 in primary cultural cells. Representative $[Ca^{2+}]_i$ traces and bar charts summarize averaged $[Ca^{2+}]_i$ peak values evoked by different concentration of Yoda1 and Yoda1 plus GsMTx4 (1μM, red text) as indicated in primary cultural human melanocytes (**A**, **A1**), isolated SCs from naïve rat sciatic nerves (**B**, **B1**), dissociated PSNs (**C**, **C1**) with dot plots (**C2**) showing correlation of Yoda1 responses to PSN sizes (small-medium size ≤ 40 diameter), DRG dissociated SGCs (**D**, **D1,** including other glia, e.g. SCs), and dissociated spinal DH glia (**E**, **E1**). The numbers on the top of scattered plots with bars are the responders (numerators) out of total cells recorded (denominators) and % of responders (brackets). Comparison of the averaged $[Ca^{2+}]_i$ peak values (scattered plots with the bars) of the responders to 1μM (**F**) and 5μM (**G**) of Yoda1 among the PSNs, SGCs, SCs, and DH glia with the numbers indicated in brackets, ***p<0.001, one-way ANOVA, Turkey *post hoc*.

Figure 7. Activation of Piezo1 in PSNs and SGCs following TNI. Scattered plots with bars summarize means±SEM of mechanical allodynia (vF) and hyperalgesia (Pin) in TNI (**A**) and

SNI (**C**) rats (n=10 for each group), ***p<0.001, unpaired two-tailed Student's t-test for vF and Mann–Whitney test for Pin. DRG homogenates were extracted from the DRG (pooled L4/L5) at 28 days after TNI (**B**) and SNI (**D**) or control (sham), and subjected to immunoblotting (IB) as shown in the representative IBs of Piezo1, Iba1, and Gapdh. The densitometry of canonical piezo1 (~300KDa) and Iba1was analyzed and summarized in bar charts (right panels of **B**, **D**); ***p<0.001, unpaired two-tailed Student's t-test. Comparison of $[Ca^{2+}]_i$ traces evoked by 1 and 10μM of Yoda1 in PSNs (**E**) and SGCs (containing other glia population) (**G**), the scattered plots with bars showing the averaged $[Ca^{2+}]_i$ peak values evoked by 1 and 10μM of Yoda1 in PSNs (**E1**) and SGCs (**G1**) from sham and TNI rats, *p<0.05, unpaired two-tailed Student's t-test. Shown in **E2** and **G2** summarize the % of responders vs. non-responders evoked by 1, 5, and 10μM of Yoda1 in PSNs (**E2**) and SGCs (**G2**) from sham and TNI rats, ***p<0.001, chi-square and Fisher's exact tests.

Figure 8. Reversal of TNI mechanical pain behavior by sciatic nerve application of GsMTx4. Scatter and line plots show time courses for the group averages of sensitivity to von Frey (**A**) and Pin (**B**) following ipsilateral subepineural sciatic nerve injection of GsMTx4 (20μg, n=1; 40μg, n=5, 100μl) or saline (n=6, 100μl), determined at day 21 after TNI. Right panels of A, B show averaged treatment area under the curve (tAUC) calculated for each individual for 2 hr period (15 min interval) following injection for von Frey and Pin tests, respectively. Behavior tests at 21d before injection were used as the treatment baseline (tBL) for tAUC calculation. ***p<0.001 for comparison to treatment tBL and, and $^{###}p$<0.001 for comparison between groups after treatment, respectively (repeated measures two-way ANOVA and Bonferroni *post-hoc* for von Frey and nonparametric analyses by Friedman's test with Dunn's *post hoc* for Pin.

**$p< 0.01$ and ***$p<0.001$ for tAUC comparison between groups (two-tailed unpaired Student's *t*-tests for vF and Mann-Whitney U test for Pin).

Table1. Primary antibodies and IgG controls used in this study

Antibody[a]	Host	Supplier/Cat#[b]	Dilution
IB4		LF/I21413	1.0μg/ml (IHC)
Piezo1	Rabbit polyclonal	Alomone/APC090	1:100 (IHC), 1:1000 (Wb)
Piezo1	Rabbit polyclonal	Proteintech/15939-1-AP	1:200 (ICC)
CGRP	Mouse monoclonal	SCB/sc57053	1:600 (IHC)
GFAP	Rabbit polyclonal	Dako/Z0334	1:1000 (IHC)
GFAP(GA5)	Mouse monoclonal	CS/3655	1:200 (IHC)
Hmgcs1	Goat polyclonal	SCB/sc32422	1:100 (IHC)
NeuN	Mouse monoclonal	Millipore/MAB377	1:50 (IHC)
PKCγ	Mouse monoclonal	SCB/sc166385	1:100 (IHC)
Tubb3	Mouse monoclonal	SCB/sc80016	1:500 (IHC)
NKA1α	Mouse monoclonal	SCB/sc514614	1:1000 (IHC)
Cav3.2	Mouse monoclonal	SCB/sc136990	1:500 (IHC)
GS	Mouse monoclonal	SCB/sc74430	1:800 (IHC)
S100	Mouse monoclonal	TF/MA5-12969	1:500 (IHC)
NF200	Mouse monoclonal	Sigma/N5389	1:1000 (IHC)
ACTA2	Mouse monoclonal	CS/56856	1:500 (IHC)
Syp	Mouse monoclonal	SCB/sc17750	1:200 (IHC)
Synpr	Mouse monoclonal	SCB/sc376761	1:200 (IHC)
CK14	Mouse monoclonal	SCB/sc53253	1:200 (IHC)
MBP	Mouse monoclonal	CS/41168	1:800 (IHC)
P75NTR	Mouse monoclonal	SCB/sc271708	1:100 (IHC)
Iba1	Rabbit polyclonal	Wako/019-19741	1:1000 (Wb)
GAPDH	Mouse monoclonal	Sigma/SAB1403850	1:5000 (Wb)
IgG control	Mouse	LF/31903	1:100~400
IgG control	Rabbit	LF/MA5-16384	1:100~1000

[a] *Antibody abbreviations: IB4, Isolectin IB4; Piezo1, Piezo type mechanosensitive ion channel component 1; CGRP, calcitonin gene-related peptide; GFAP, Glial fibrillary acidic protein; Hmgcs1, 3-hydroxy-3-methylglutaryl coenzyme A synthase-1; NeuN, Neuronal nuclear protein; PKCγ, Protein kinase C gamma*; *Tubb3, β3-Tubulin; NKA1α, sodium/potassium ATPase 1α; Cav3.2, T-type calcium channel 3.2α1H; GS, glutamine synthetase; S100, S100 calcium binding protein; NF200, neurofilament-200; ACTA2, α-Smooth muscle actin*; *Syp, synaptophysin; Synpr, synaptoporin; CK14, cytokeratin 14; MBP, myelin basic protein; P75NTR, neurotrophin receptor p75; Iba1, allograft inflammatory factor-1; GAPDH, glycolytic enzyme glyceraldehyde-3-phosphate dehydrogenase.*

[b] *LF, Life Technologies, Carlsbad, CA; Alomone, Alomone Labs, Jerusalem, Israel; Proteintech, Rosemont, IL; SCB, Santa Cruz Biotechnology, Santa Cruz, CA; Millipore, Burlington, MA; CS, Cell signaling, Danvers, MA; Wako, Richmond, VA; Dako: Carpinteria, California; Sigma, Sigma-Aldrich, St Louis, MO.*

Figure 1

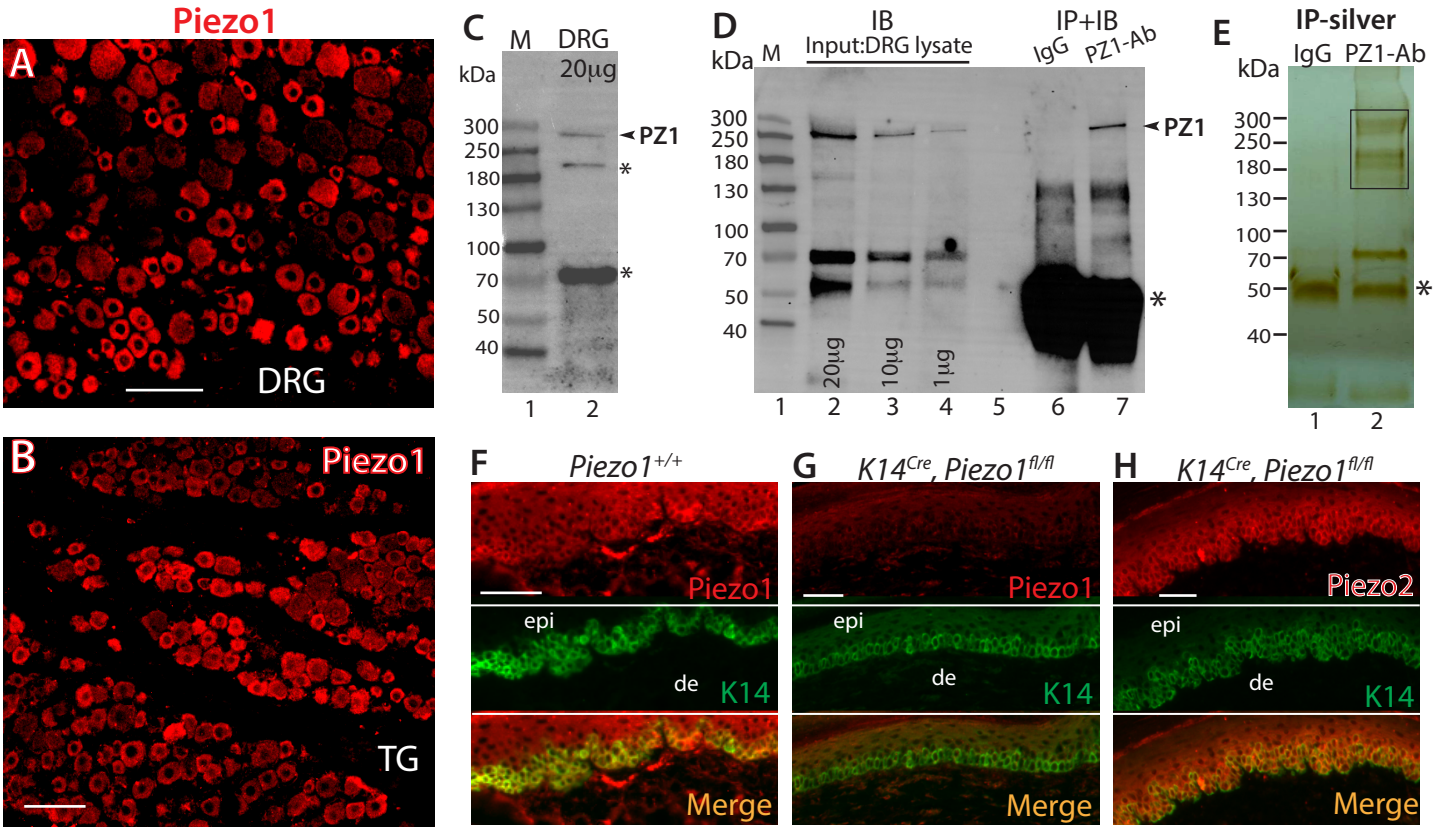

Figure 2

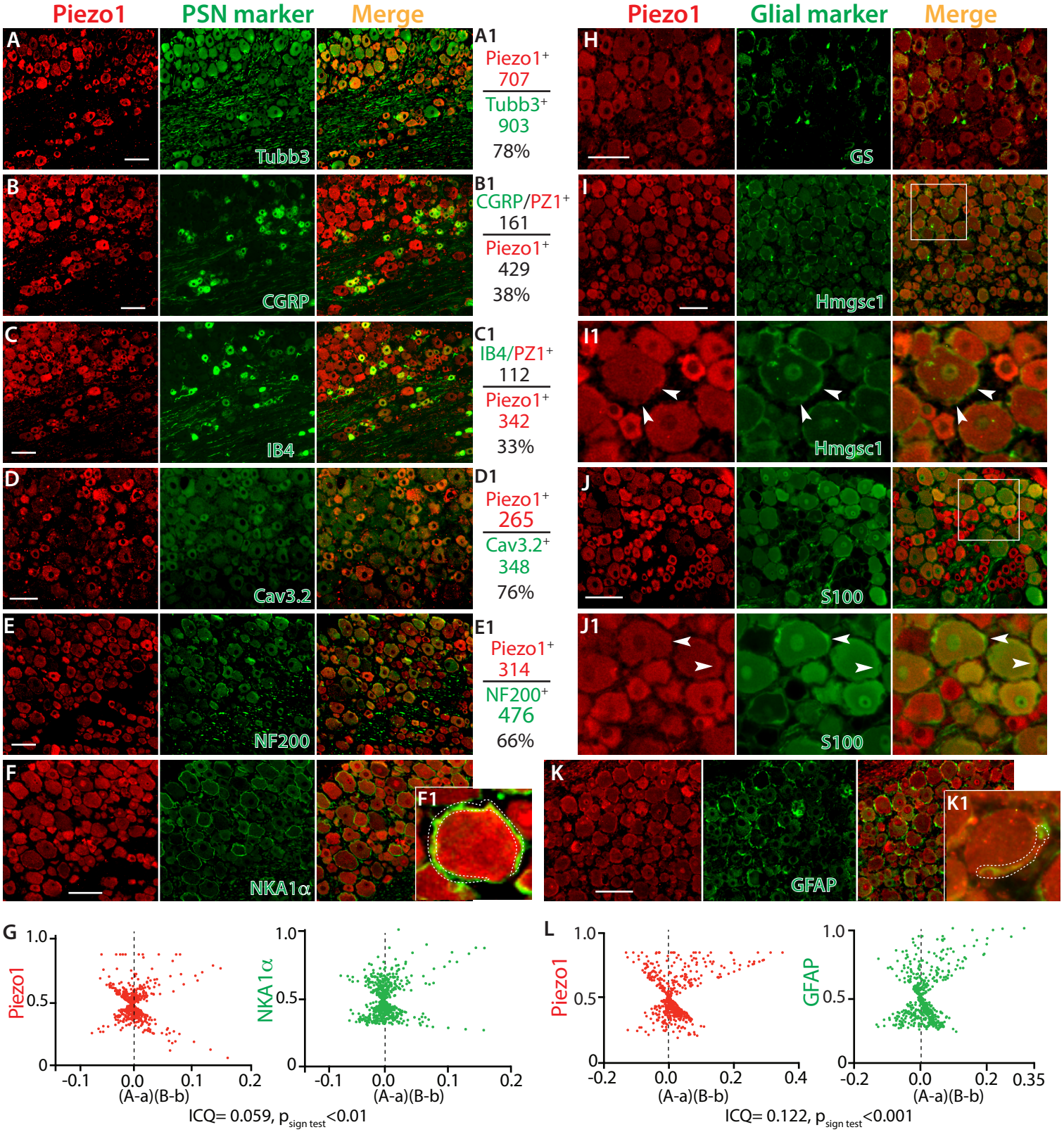

Figure 3

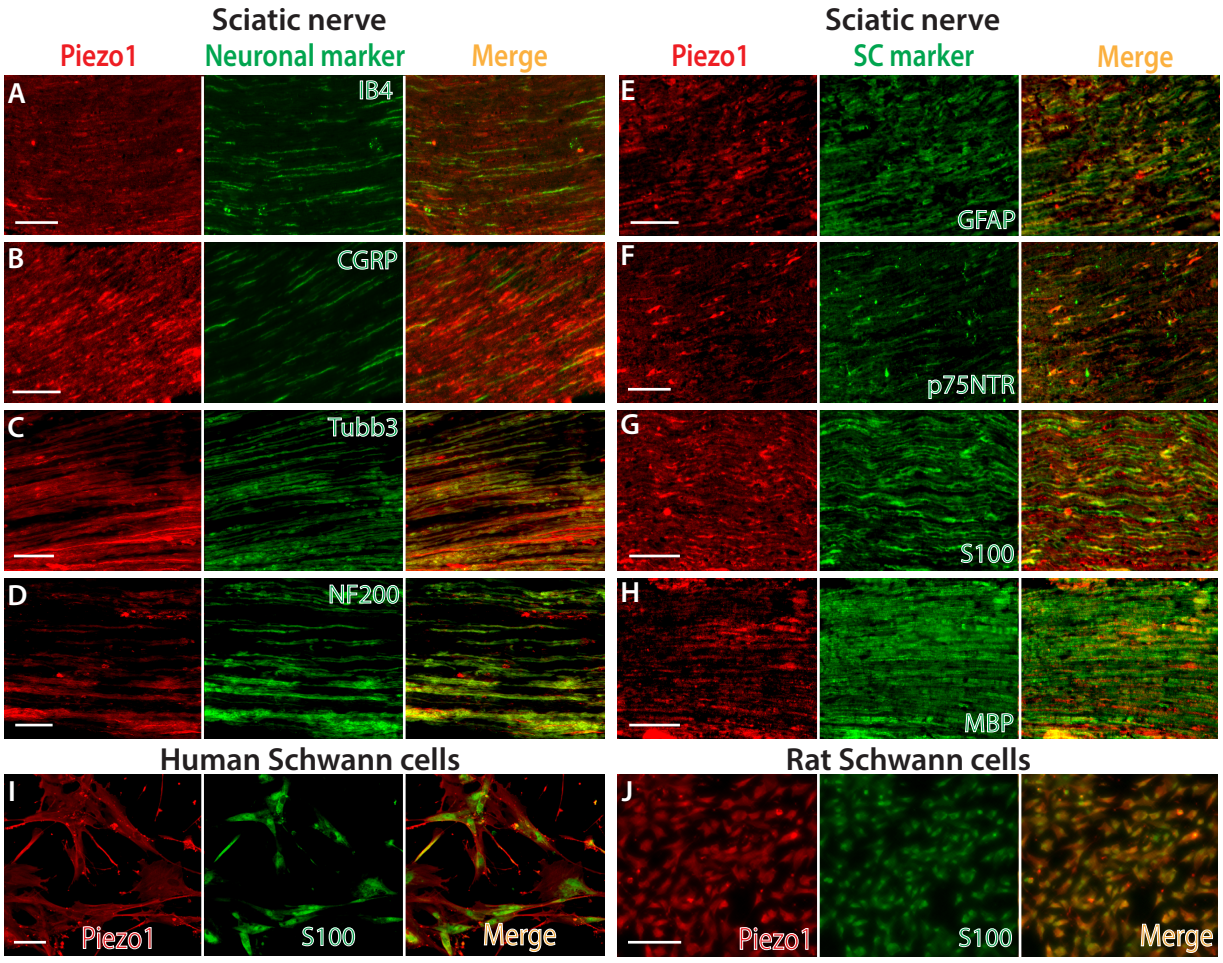

Figure 4

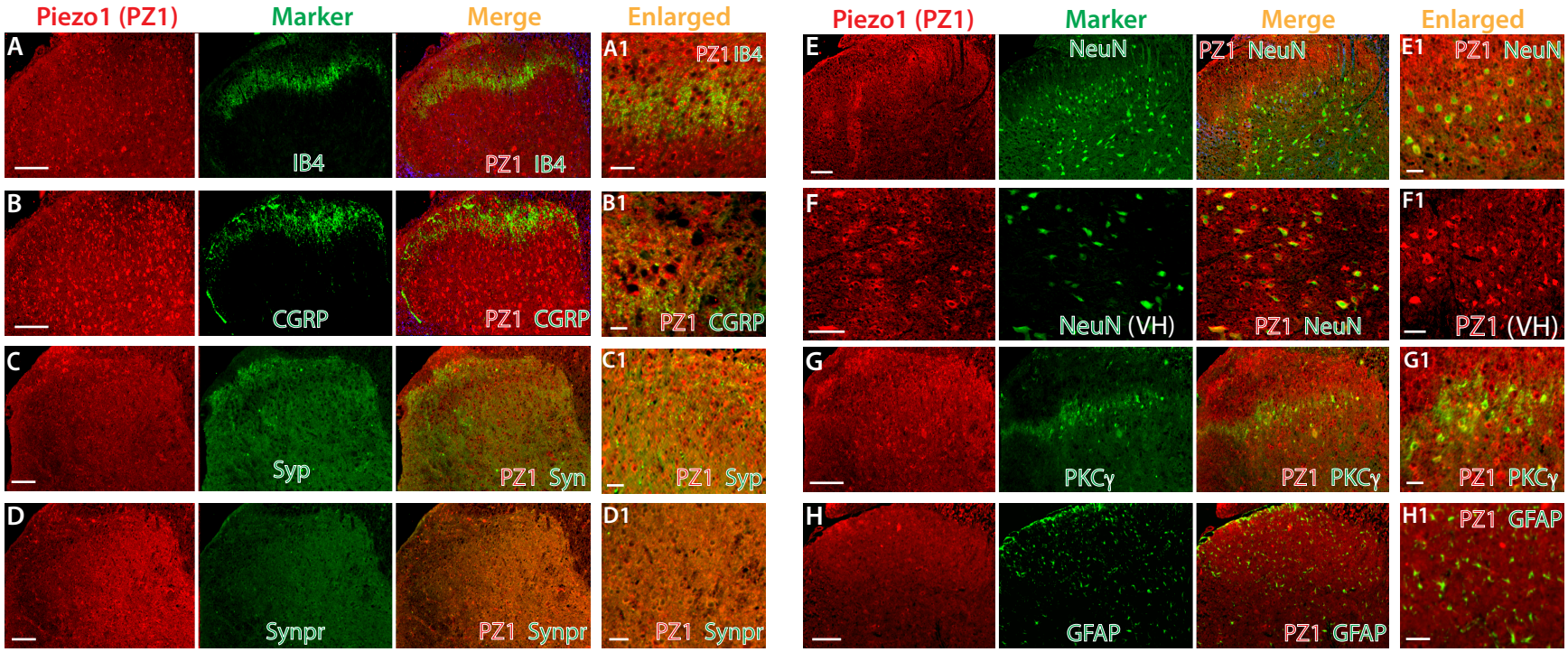
Piezo1 (PZ1)
Marker
Merge
Enlarged
A
IB4
PZ1 IB4
A1
PZ1 IB4
B
CGRP
PZ1 CGRP
B1
PZ1 CGRP
C
Syp
PZ1 Syn
C1
PZ1 Syp
D
Synpr
PZ1 Synpr
D1
PZ1 Synpr
Piezo1 (PZ1)
Marker
Merge
Enlarged
E
NeuN
PZ1 NeuN
E1
PZ1 NeuN
F
NeuN (VH)
PZ1 NeuN
F1
PZ1 (VH)
G
PKCγ
PZ1 PKCγ
G1
PZ1 PKCγ
H
GFAP
PZ1 GFAP
H1
PZ1 GFAP

Figure 5

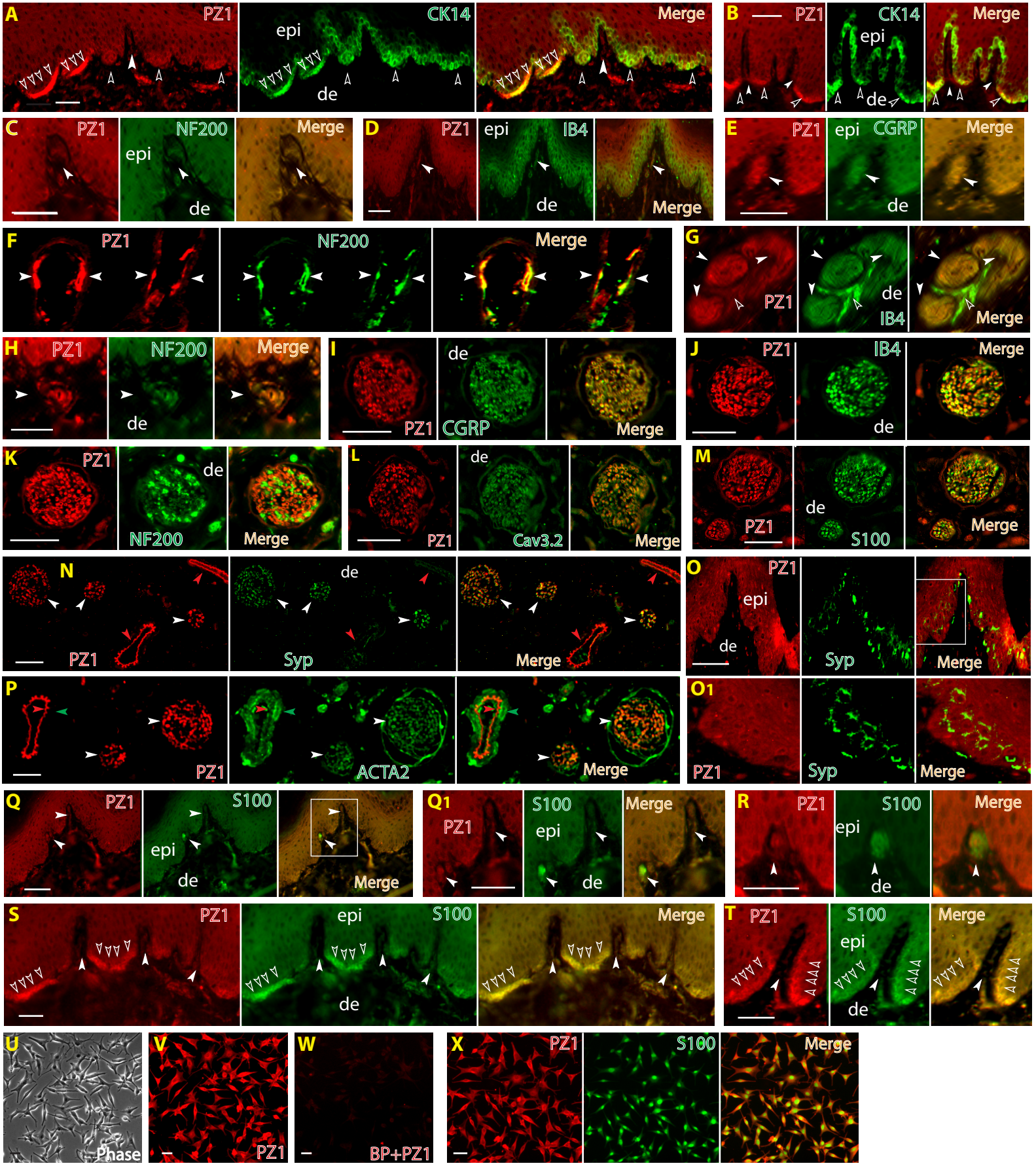

Figure 6

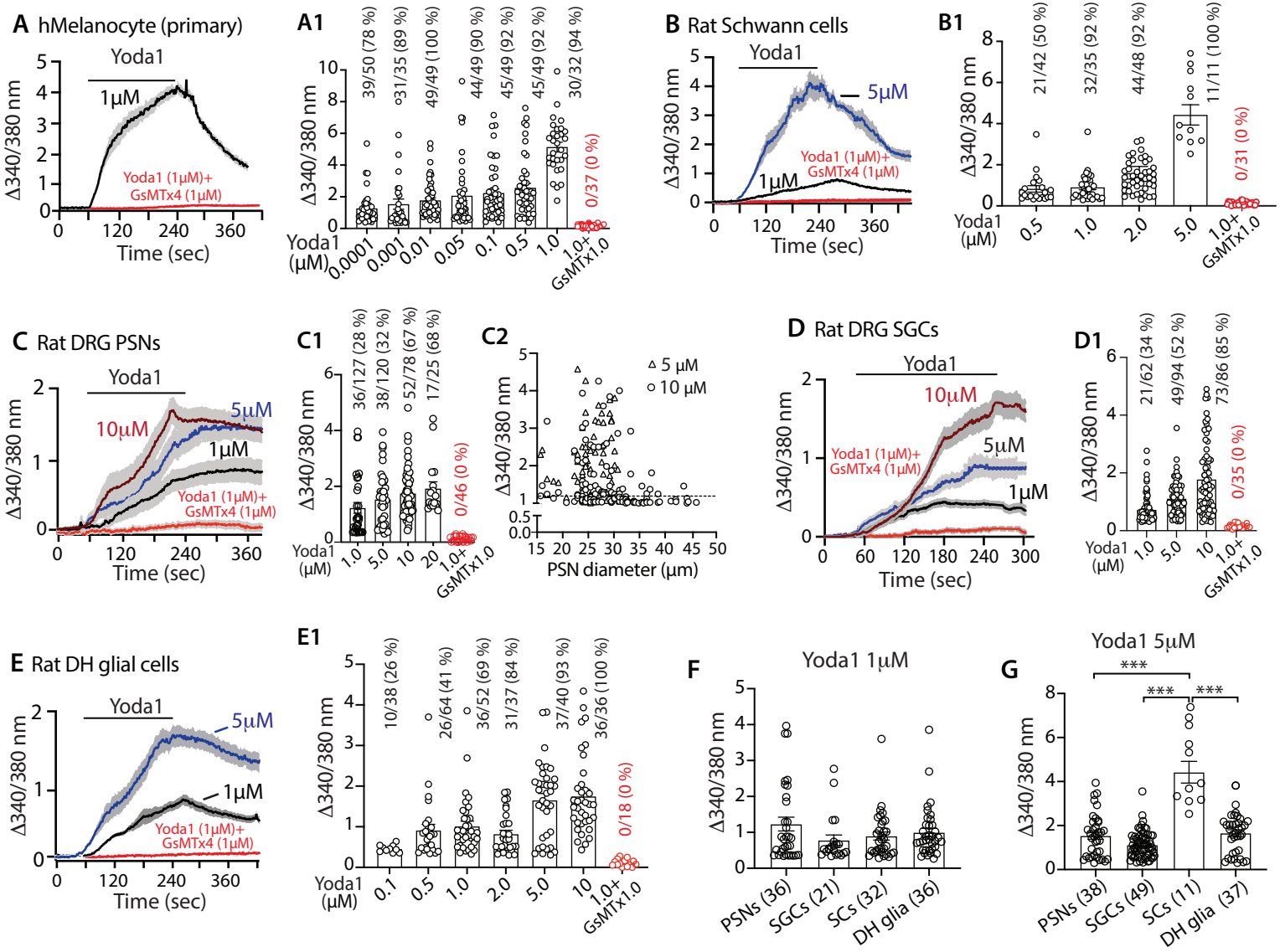
A hMelanocyte (primary)
Yoda1
1μM
Yoda1 (1μM)+ GsMTx4 (1μM)
Δ340/380 nm
Time (sec)
A1
39/50 (78 %)
31/35 (89 %)
49/49 (100 %)
44/49 (90 %)
45/49 (92 %)
45/49 (92 %)
30/32 (94 %)
0/37 (0 %)
Yoda1 (μM)
0.0001
0.001
0.01
0.05
0.1
0.5
1.0
1.0+ GsMTx1.0
B Rat Schwann cells
Yoda1
5μM
1μM
Yoda1 (1μM)+ GsMTx4 (1μM)
Time (sec)
B1
21/42 (50 %)
32/35 (92 %)
44/48 (92 %)
11/11 (100 %)
0/31 (0 %)
C Rat DRG PSNs
Yoda1
10μM
5μM
1μM
Yoda1 (1μM)+ GsMTx4 (1μM)
Time (sec)
C1
36/127 (28 %)
38/120 (32 %)
52/78 (67 %)
17/25 (68 %)
0/46 (0 %)
C2
5 μM
10 μM
PSN diameter (μm)
D Rat DRG SGCs
Yoda1
10μM
5μM
1μM
Yoda1 (1μM)+ GsMTx4 (1μM)
Time (sec)
D1
21/62 (34 %)
49/94 (52 %)
73/86 (85 %)
0/35 (0 %)
E Rat DH glial cells
Yoda1
5μM
1μM
Yoda1 (1μM)+ GsMTx4 (1μM)
Time (sec)
E1
10/38 (26 %)
26/64 (41 %)
36/52 (69 %)
31/37 (84 %)
37/40 (93 %)
36/36 (100 %)
0/18 (0 %)
F
Yoda1 1μM
PSNs (36)
SGCs (21)
SCs (32)
DH glia (36)
G
Yoda1 5μM
***
***
***
PSNs (38)
SGCs (49)
SCs (11)
DH glia (37)

Figure 7

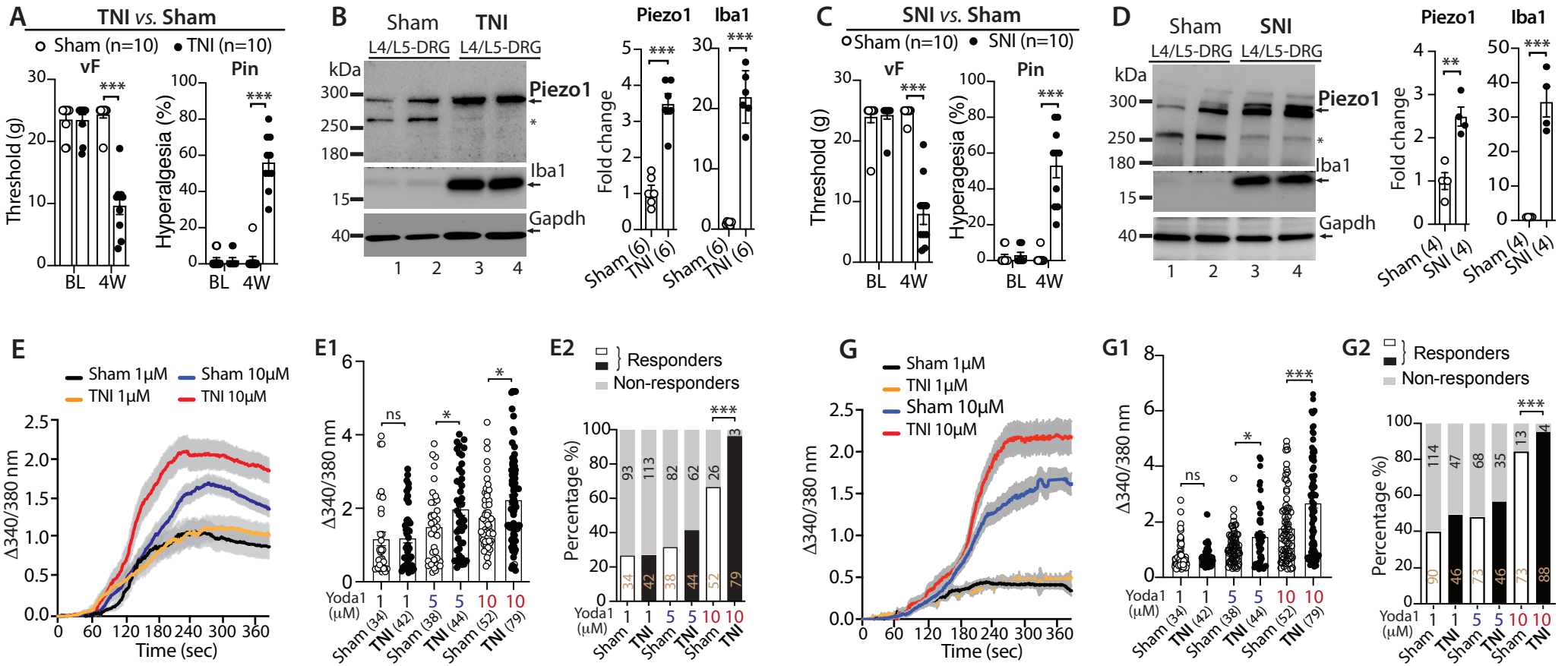
A
TNI vs. Sham
Sham (n=10)
TNI (n=10)
vF
Pin
Threshold (g)
Hyperalgesia (%)
BL
4W
B
Sham
TNI
L4/L5-DRG
kDa
Piezo1
Iba1
Gapdh
Fold change
C
SNI vs. Sham
SNI (n=10)
D
SNI
E
Sham 1μM
Sham 10μM
TNI 1μM
TNI 10μM
Δ340/380 nm
Time (sec)
E1
E2
Responders
Non-responders
Percentage %
Yoda1 (μM)
G
G1
G2

Figure 8

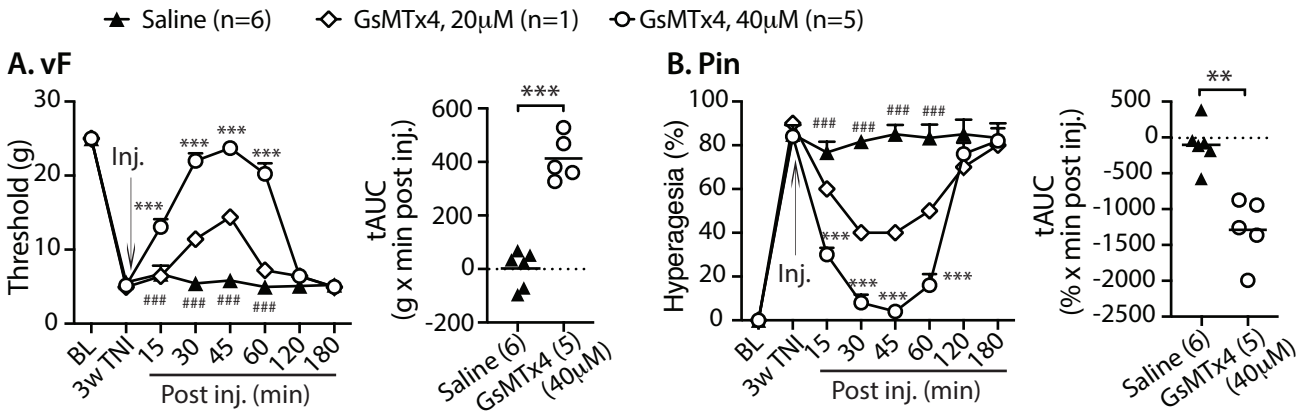

Supplementary Figures

Peripheral sensory neurons and non-neuronal cells express functional Piezo1 that is activated in peripheral nerve injury-induced neuropathic pain

Abbreviated Title: Peripheral nerve Piezo1 is activated following neuropathic pain

Seung Min Shin, Brandon Itson-Zoske, Fan Fan, Cheryl L. Stucky, Quinn H. Hogan, and Hongwei Yu

A

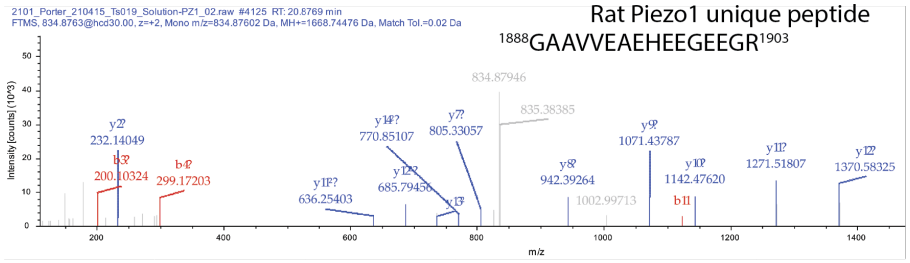

B

#1	b⁺	b²⁺	Seq.	y⁺	y²⁺	#2
1	58.02874	29.51801	G			16
2	129.06585	65.03657	A	1611.72452	806.36590	15
3	200.10297	100.55512	A	1540.68740	770.84734	14
4	299.17138	150.08933	V	1469.65029	735.32878	13
5	398.23980	199.62354	V	1370.58188	685.79458	12
6	527.28239	264.14483	E	1271.51346	636.26037	11
7	598.31950	299.66339	A	1142.47087	571.73907	10
8	727.36210	364.18469	E	1071.43376	536.22052	9
9	864.42101	432.71414	H	942.39116	471.69922	8
10	993.46360	497.23544	E	805.33225	403.16976	7
11	1122.50619	561.75673	E	676.28966	338.64847	6
12	1179.52766	590.26747	G	547.24707	274.12717	5
13	1308.57025	654.78876	E	490.22560	245.61644	4
14	1437.61284	719.31006	E	361.18301	181.09514	3
15	1494.63431	747.82079	G	232.14042	116.57385	2
16			R	175.11895	88.06311	1

Figure S1. Identification of DRG Piezo1 from naïve rats using immunoprecipitation and mass spectroscopy. Representative ion chromatography (**A**) and MS/MS spectrum of *m/z* distributions of Piezo1 peptide **(B)** obtained after excision of silver-stained protein bands from ~150-320 kDa in SDS-PAGE gel of Piezo1 CO-IP sample (Fig. 1) prepared from DRG of naïve rats. MS/MS (tandem mass spectrometry) was carried out on the peptide mixture obtained from in-gel digestion of SDS-PAGE separated protein samples with LCQ ion trap mass spectrometer on-line coupled with an HPLC with 75-μm i.d. C18 column. The precursor ions were selected automatically by the instrument. The peptide sequence was identified by bioinformatics analysis and found to correspond to the parent rat protein Piezo1.

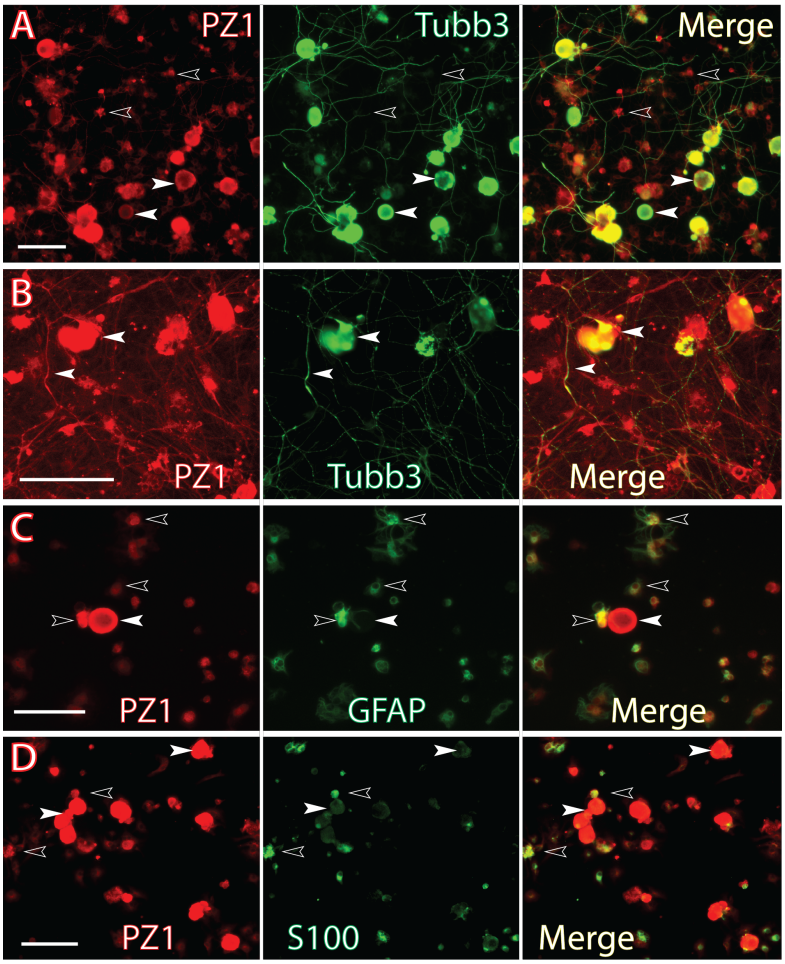

Figure S2. ICC of Piezo1 (PZ1) in DRG dissociated culture.
Representative montage images of Piezo1-IR by ICC on DRG dissociated culture at Days In Vitro (DIV) =3 show Piezo1 (red) in neuronal somata and their axons (white arrowheads), as well as smaller glia-like cells and their neurites (empty arrowheads) (**A, B**). Representative montage images of ICC double immunostaining on DRG dissociated culture (DIV=0.25) show Piezo1 (red, white arrowheads) immunopositivity in neurons and co-stained with GFAP-positive (green, empty arrowheads) (**C**) and S100-positive glia cells (**D**). Scale bars: 100 μm for all.

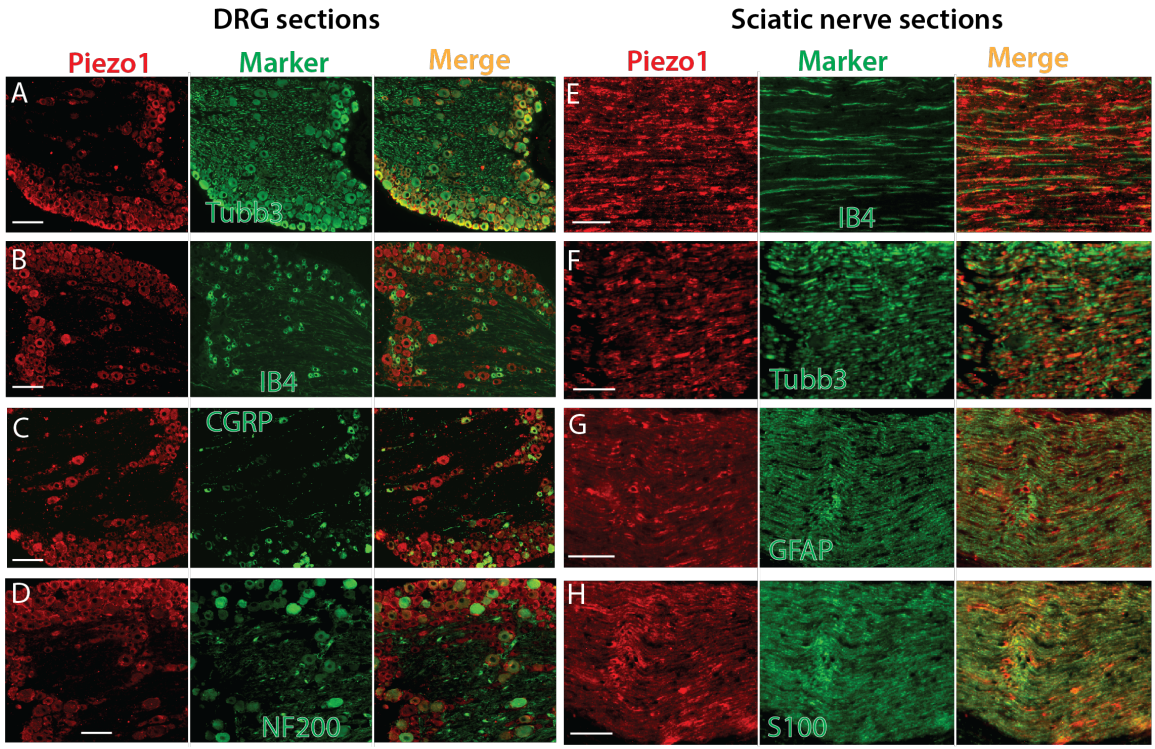

Figure S3. **IHC detection of Piezo1 in mice DRG and sciatic nerve.** In DRG sections from wild-type (WT) mice, Piezo1 antibody (Alomone) detected neuronal profile of Piezo1 expression, showing Piezo1-IR (red) co-stained with neuronal markers (green), including Tubb3 (**A**), IB4 (**B**), CGRP (**C**), and NF200 (**D**). In sciatic nerve sections from WT mice, Piezo1-IR (red) was detected neuronal profile of Piezo1 expression, showing Piezo1-IR (red) co-stained with neuronal markers IB4 (**E**) and Tubb3 (**F**) (green), as well as Schwann cell markers GFAP (**G**) and S100 (**H**) (green). Scale bars: 50 μm for all.

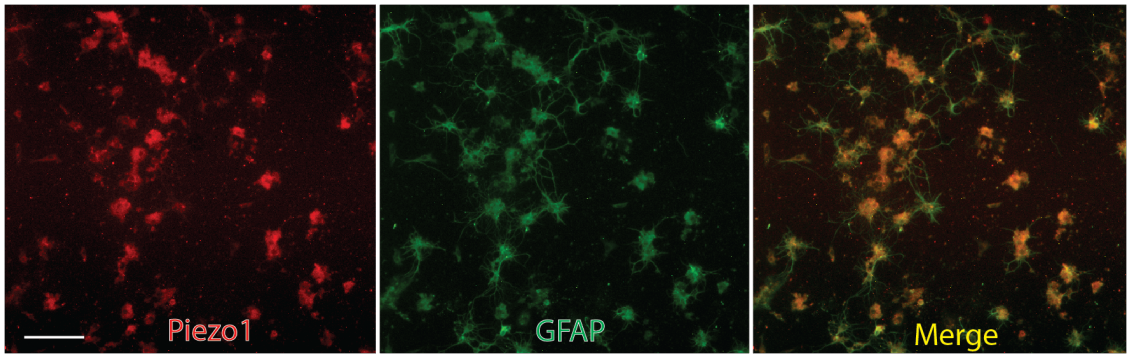

Figure S4. Colocalization of Piezo1 and GFAP in spinal DH dissociated glia cultures. Shown are IHC montage images of Piezo1 (red), GFAP (green), displaying colabeling (merged image) on rat spinal DH glial cell culture (DIV=4 days) after dissociation. Scale bar: 50µm

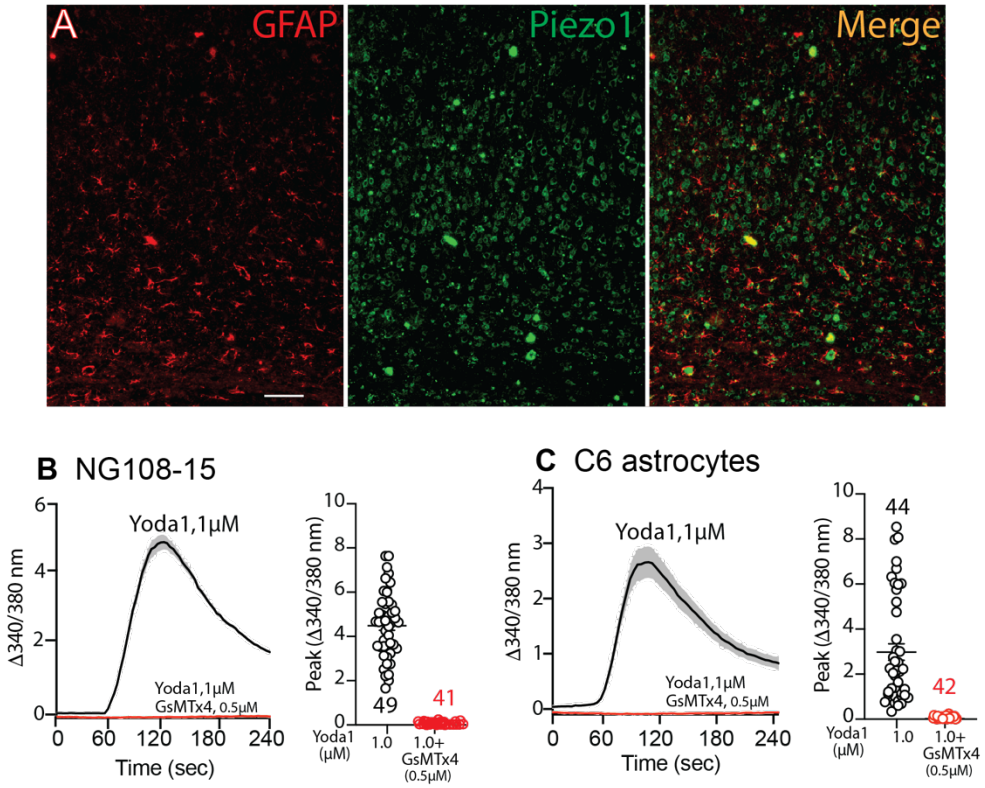

Figure S5. Detection Piezo1 expression in brain neurons and astrocytes. Representative IHC montage images (**A**) display immunostaining of Piezo1 (red) with GFAP (green), showing Piezo1 and GFAP colabeling (yellow) in merged image on a section of the brain cerebral cortex areas of naïve adult rat. Scale bar: 50µm. Averaged $[Ca^{2+}]_i$ traces and scattered plots $[Ca^{2+}]_i$ peak values with means (lines) of Fura-2 fluorometric Ca^{2+} imaging of NG108-15, mice brain cortex neuronal cells (**A**) and C6 rat brain astrocytes (**B**). Ca^{2+} entry was evoked by 1µM Yoda1 which was blocked by addition of 1µM GsMTx4 (red traces).

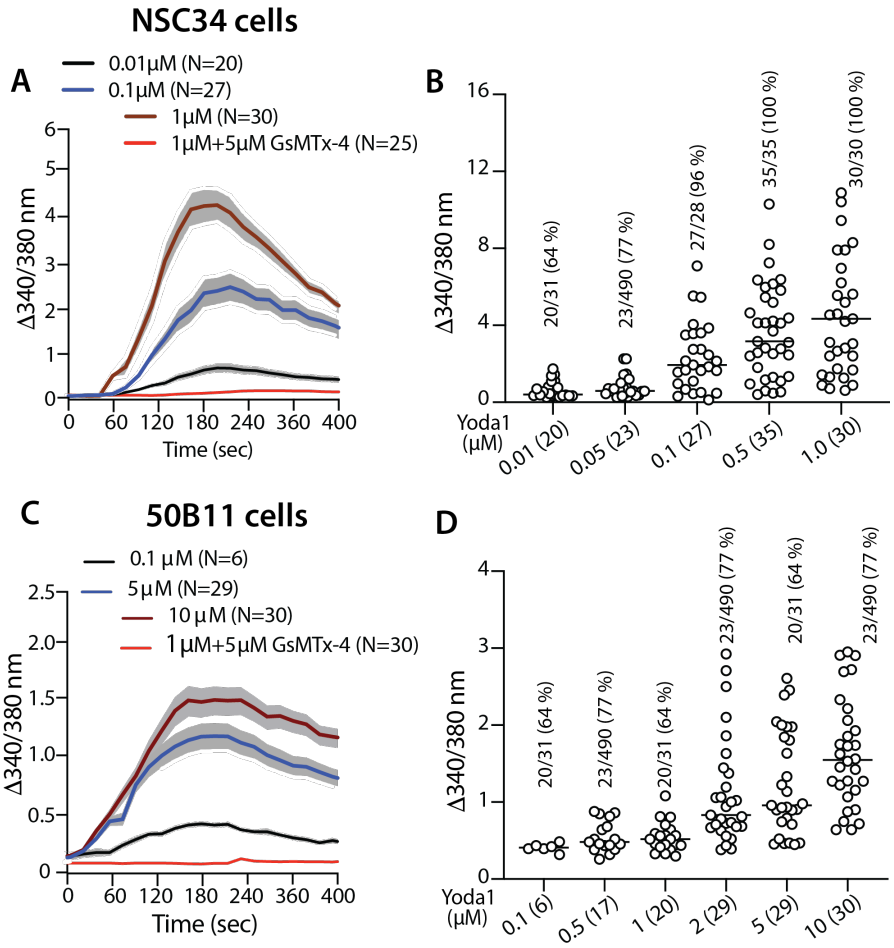

Figure S6. Functional Piezo1 in NSC34 and 50B11 cells. Representative $[Ca^{2+}]_i$ traces (**A**) and scattered plots (**B**) summarize the averaged $[Ca^{2+}]_i$ peak values evoked by different concentration of Yoda1 and Yoda1 (1μM) plus GsMTx4 5μM) as indicated in the cultural NSC34 spinal motor neuron-like cells. The numbers on the top of scattered plots with the mean (lines) are the responders (numerators) out of total cells recorded (denominators) and % of responders (brackets). Representative $[Ca^{2+}]_i$ traces (**C**) and scattered plots (**D**) summarize averaged $[Ca^{2+}]_i$ peak values evoked by different concentration of Yoda1 and Yoda1 (1μM) plus GsMTx4 5μM) as indicated in the cultural rat DRG neuronal 50B11 cells. The numbers on the top of scattered plots with the mean (lines) are the responders (numerators) out of total cells recorded (denominators) and % of responders (brackets).